Research Article

Pathogenic neutrophilia drives acute respiratory distress syndrome in severe COVID-19 patients

Running title: Pathogenic airway neutrophilia in severe COVID-19

Devon J. Eddins[1,2,3], Junkai Yang[1,†], Astrid Kosters[1,†], Vincent D. Giacalone[2,4], Ximo Pechuan[5], Joshua D. Chandler[2,4], Benjamin R. Babcock[1], Jinyoung Eum[1,6], Mindy R. Hernández[7], Fathma Abdulkhader[1], Genoah L. Collins[2,4], Richard P. Ramonell[7], Christine Moussion[6], Darya Y. Orlova[6], Ignacio Sanz[1,3,8], F. Eun-Hyung Lee[1,3,7], Rabindra M. Tirouvanziam[2,4], Eliver E.B. Ghosn[1,2,3,6*]

[1]Lowance Center for Human Immunology, Department of Medicine, Division of Immunology and Rheumatology, Emory University School of Medicine, Atlanta, GA 30322, USA

[2]Department of Pediatrics, Emory University School of Medicine, Atlanta, GA 30322, USA

[3]Emory Vaccine Center, Yerkes National Primate Research Center, Emory University School of Medicine, Atlanta, GA 30322, USA

[4]Center for CF & Airways Disease Research, Children's Healthcare of Atlanta, Atlanta, 30322 GA, USA

[5]Genentech, Inc., South San Francisco, California 94080, USA

[6]Georgia Institute of Technology, Bioinformatics Graduate Program, Atlanta, GA 30332, USA

[7]Division of Pulmonary, Allergy, Critical Care & Sleep Medicine, Department of Medicine, Emory University School of Medicine, Atlanta, GA 30322, USA

[8]Emory Autoimmunity Center of Excellence, Department of Medicine, Division of Rheumatology, Emory University School of Medicine, Atlanta, GA 30322, USA

[†]Contributed equally

Corresponding Author Contact Info

Eliver E.B. Ghosn (ORCID: 0000-0001-7258-906X): Lowance Center for Human Immunology, Health Sciences Research Building, 1760 Haygood Dr. NE, E240, Atlanta, GA 30322, USA; tel: +1-404-712-3211; email: eliver.ghosn@emory.edu

Abstract

Severe acute respiratory syndrome coronavirus 2 (SARS-CoV-2) and the ensuing COVID-19 pandemic have caused ~33 million cases and over 585,000 deaths in the United States alone. Troubling disparities in COVID-19-associated mortality emerged early, with nearly 70% of deaths being Black/African-American (AA) patients in some areas, yet targeted studies to delineate features of disease severity within this demographic are scant. Our multi-omics single-cell analyses of immune profiles from airways and matching blood samples of Black/AA patients revealed pronounced pulmonary neutrophilia and low viral burden as a hallmark of severe disease, where neutrophil phenotypes display advanced features of cytokine release syndrome and acute respiratory distress syndrome (ARDS). Cell-cell communication and trajectory analysis reveal a subset of circulating S100A12^{+}/CXCR4^{+} mature neutrophils that infiltrate the lung via the IL-8/CXCR2 axis. Recruited neutrophils progress toward a transcriptionally active and pathogenic state characterized by exacerbated production of IL-8, IL-1β, IL-6, and CCL3/4 along with elevated levels of neutrophil elastase and myeloperoxidase. Inflammatory monocytes recruited via neutrophil-derived CCL3/4 also produce elevated neutrophil chemotactic factor IL-8, potentiating the sustained neutrophilia in the airways. The IL-8/CXCR2 axis emerges as a potential therapeutic target to reduce pathogenic neutrophilia and constrain ARDS in severe COVID-19.

Introduction

The coronavirus disease 2019 (COVID-19) pandemic, caused by SARS-CoV-2, is associated with high morbidity and mortality. To date, the pandemic has caused ~33 million cases and over 585,000 deaths in the United States alone, where communities of color are disproportionately burdened with disease severity and mortality[1]. A hallmark of COVID-19 pathogenesis is the vast array of clinical presentations and outcomes, which range from asymptomatic or a mild, self-limiting disease to acute respiratory distress syndrome (ARDS), multiorgan failure, and death. Indeed, such diversity in COVID-19 pathogenesis poses challenges to identify processes that dictate progression to severe disease. Early reports highlighted systemic hyperinflammatory responses that are linked to disease severity[2]. Cytokine release syndrome, also called a cytokine storm, has been observed in many patients and is suspected of causing the detrimental progression of COVID-19 and sustained immune dysregulation[3].

Severe COVID-19 disease parallels the pathophysiology of sepsis[4], where clinical presentation often includes granulocytosis, elevated proinflammatory cytokine production, aberrant myeloid activation, altered dendritic cell (DCs) population dynamics, and lymphopenia[5, 6]. Early single-cell analyses of bronchoalveolar lavage samples implicated dysregulated monocyte and macrophage responses as central features in poor outcomes[3, 7]. As such, most early efforts have been focused on characterizing and constraining aberrant monocyte/macrophage responses. Concurrently, reports of neutrophilia in the peripheral blood arose, and the neutrophil to lymphocyte ratio emerged as an independent risk factor for disease progression[8]. Interestingly, a prior investigation of ARDS following sepsis identified sustained neutrophilia associated with worsened prognosis and death in comparison to patients who resolved neutrophilia and showed an increase in tissue-resident alveolar macrophages[9], which may present another shared feature between COVID-19 and sepsis.

To date, there have been many studies of neutrophil responses in the blood of COVID-19 patients[10, 11, 12]. However, an in-depth analysis of the neutrophil activity in the lungs is lacking. Expressly, the extent to which neutrophils contribute to cytokine release syndrome, tissue damage, and ultimately ADRS in severe COVID-19 cases is incompletely understood. Our systems immunology approach, combining high-dimensional (Hi-D, 30-parameter) flow cytometry and multi-omics single-cell sequencing analyses of immune profiles from the airways and matching blood samples of Black/AA patients, revealed pronounced and sustained pulmonary neutrophilia as a hallmark of severe disease. Mature pulmonary neutrophils produce very high levels of the neutrophil chemotactic factor IL-8 in addition to IL-1β, IL-6, and CCL3/4 along with copious amounts of neutrophil elastase (NE) and myeloperoxidase (MPO). Altogether, our findings highlight that transcriptionally active and highly inflammatory neutrophils are sustained in the airways of critically ill patients and that reducing pathogenic neutrophilia may constrain ARDS in severe COVID-19 disease.

Results

Study Cohort

To better understand immune dynamics in Black/African-American (AA) patients with severe COVID-19, we analyzed airway and matching blood samples from a cohort of 35 individuals presenting to Emory University Hospitals (severe) or the Emory Acute Respiratory Clinic (mild-acute) in Atlanta, GA, USA (Fig. 1 & Table S1), including 8 demographic-matched healthy adults as controls. Of the 27 individuals who were confirmed positive by PCR from nasopharyngeal swabs, 18 had an NIH severity score of “critical” (referred to as severe herein) and were admitted to the intensive care unit (ICU) requiring mechanical ventilator support and 9 were mild (mild-acute) outpatients. All severe patients in our cohort received corticosteroids (Dexamethasone or equivalent). Approximately half received one or more doses of the antiviral medication Remdesivir, with an average ICU stay of 26 days (see Table S1).

Exacerbated neutrophilia in the airways and matching blood of severe COVID-19 patients

We first characterized major immune lineages in the airways and matching blood samples by Hi-D flow cytometry and observed a pronounced circulating neutrophilia and lymphopenia (notably T and NK cells), which is similarly reflected in the airways (Fig. 2a-d). This is in line with recent reports showing lymphopenia associated with significant alterations in the myeloid compartment[13, 14]. Strikingly, in most cases of severe disease, ≥85% of all pulmonary leukocytes were neutrophils (Fig. 2a-b). This stands in contrast to other studies which have reported much more heterogeneity in neutrophil frequency in the blood and lungs of patients[15, 16]. Circulating T cells and NK cells are decreased with increased disease severity (Fig. 2b & 2d), which has recently been reported as a feature of COVID-19 pneumonia[17]. We also observed a notable decrease in pulmonary NK cells associated with disease severity (Fig. 2b). However, there were only subtle differences in the B-cell compartment (which were detected at very low levels in the airways) and myeloid-derived cells (MdCs) compartment compared to other reports[7, 18, 19], highlighting the importance of neutrophilia and neutrophil-to-lymphocyte ratio in our cohort. Interestingly, the patient with the lowest neutrophil frequency in the airways corresponds to the youngest patient in the severe disease group (Fig. 2b). However, since we only had a single patient under the age of 35 in our severe group, we cannot conclude any associations between neutrophilia and patient age.

Since we identified a prominent neutrophilia in our cohort, we developed a Hi-D, 30-parameter flow cytometry panel to interrogate inflammatory neutrophil phenotype in addition to broad leukocyte characterization (see “CoV-Neutrophil” panel in Table S2). Here, we used extracellular staining of NE and CD63 (LAMP3) to assess primary granule release[20], coupled with intracellular staining for key effectors implicated in cytokine storm (IL-1β, IL-6, IL-8). We observed that nearly all neutrophils recruited to the lung developed an inflammatory profile characterized by exacerbated levels of NE and elevated production of IL-1β and IL-8 with a dramatic increase in granule release (Fig. 2e-j). This phenotype is diminished in the circulation where a smaller proportion of neutrophils are undergoing granule release, and the cytokine

signature is limited mainly to IL-1β production and less IL-6 and IL-8 (Fig. 2g-k). Together, these results demonstrate systemic neutrophilia in severe COVID-19 patients where neutrophils accumulating in the airways are producing exacerbated levels of potentially damaging enzymes (e.g., NE) and inflammatory cytokines (IL-8, IL-1β) and undergoing pronounced granule release.

Neutrophil-secreted inflammatory molecules in the airways potentiate the acute respiratory distress syndrome in severe patients.

To better understand the inflammatory signaling milieu and relate the intracellular cytokine staining to the protein secretion, we measured 21 total analytes in the airways and plasma using the Mesoscale UPLEX platform. We found that CXCL8 (IL-8) is the most abundant chemokine in the airways of severe patients accompanied by high levels of IL-1β and IL-6 (Fig. 3a), which is in line with our Hi-D flow cytometry data showing neutrophilia and pronounced intracellular staining signal for IL-8 and IL-1β (see Fig. 2a-f). Strikingly, IL-8 levels were ~100-fold higher in the airways of severe versus mild patients and that of IL-1β and IL-6 levels in severe patients. These data implicate IL-8 signaling in the prominent neutrophilia observed in severe patients in our cohort.

We noticed only minor differences in circulating levels of many targets between healthy individuals and those affected by severe COVID-19 disease suggesting an uncoupling of local versus systemic inflammatory responses, particularly for IL-8 and IL-1β, but also IL-6 to a lesser extent (Fig. 3a). Conversely, we did observe a rise in circulating IL-1RA levels with increasing disease severity, but not in the respiratory secretions. This is in stark contrast to IL-1β levels which were not markedly difference in the circulation but significantly increased in the airways in severe disease. We also found increased CCL2 (MCP-1) in the airways of severe disease, and the same trend for M-CSF and TNF was observed, albeit at much lower concentrations (Fig. 3a). IFN-γ was detected at the highest levels in the airways of severe patients with no obvious differentiation in plasma across all groups. IL-10 was also increased in the airways of severe patients with notable variation at low levels (Fig. 3a). In contrast to other studies, we did not observe appreciable differences in IL-18 or CXCL10 (IP-10) levels across patient groups (Fig. S1). CXCL12 was detected at higher levels in the airways of severe patients, although in some patients, the levels were below the limit of the detection for the assay, suggesting a wide distribution for this ligand (Fig. S1).

We further measured the neutrophil-derived myeloperoxidase (MPO) protein concentrations and their enzymatic activity across patient groups. MPO is an important neutrophil effector molecule originating from the same granules as NE that has been implicated in respiratory illnesses such as cystic fibrosis[21], and can contribute to lung tissue damage during neutrophilic pneumonitis. MPO protein concentrations increase in a stepwise manner with disease severity in both the plasma and respiratory supernatant (Fig. 3b). However, MPO activity is mostly detected in the airways, with an increase in MPO activity with increasing disease severity (Fig. 3b).

Recruited airway neutrophils are mature, transcriptionally active, and further differentiate into a highly inflammatory state

A prior study had reported an increase in immature neutrophils in the lung concomitant to increased circulating immature neutrophils in the form of emergency hematopoiesis in severe COVID-19 patients[14]. We, therefore, assessed the immature neutrophil phenotype by scRNA-seq in our patient cohort. We readily identified a cluster of neutrophils expressing *CAMP*, *LTF*, *RETN*, *OLFM4*, *DEFA3*, *CD24*, and *MMP8* (Fig. 4e & S2) in the blood of severe patients (cluster 3 in blood neutrophils), that also has high expression of calprotectin (S100A8/9) and other calgranulins. This is consistent with immature neutrophil phenotypes described by others[13] and was notably absent in neutrophils from the lung (Fig. 4j), suggesting that immature neutrophils are not directly recruited to the lung or they quickly differentiate upon lung infiltration.

To determine whether immature neutrophils can infiltrate the lung and further differentiate into a pathogenic state, we explored the chemokine receptors known to promote neutrophil chemotaxis to the lung, such as the IL-8 receptor CXCR2. Our finding that IL-8 was increased in neutrophils by flow cytometry (Fig. 2) and also present at very high levels in the respiratory supernatant (Fig. 3) suggests that the IL-8/CXCR2 signaling axis is important for neutrophil recruitment to the lungs during COVID-19 pathogenesis. Surprisingly, the immature neutrophils (cluster 3) lacked *CXCR2* (Fig. 5c), suggesting that immature neutrophils are unlikely to infiltrate the lung via IL-8. In contrast, a defined subset of mature neutrophils in blood expresses high levels of *CXCR2* along with *CXCR4* and *S100A12* (Fig. 2d & S3), identifying the blood cluster 2 as the neutrophil subset that can infiltrate the lung via IL-8 (Figs. 4d & 5c). It is, therefore, probable that recent lung immigrants would still express detectable levels of *CXCR2* as well as *CXCR4* and *S100A12* (Figs. 4d & 5c).

Indeed, when we investigated the expression levels of *CXCR2* and *S100A12* in the lung, we identified neutrophil cluster 0 as the putative immigrant population from the blood (i.e., circulating neutrophil cluster 2 likely infiltrate the lung and acquire the phenotype of neutrophil cluster 0) (Fig. 5c). After identifying the lung neutrophil cluster 0 as the putative emigrant population from the blood, we sought to identify their cell trajectory/differentiation once they enter the inflamed airway. Cell trajectory analyses (Slingshot) revealed two differentiation pathways (Trajectories 1 and 2) for the recently infiltrated neutrophils (see blue arrows in Fig. 5c). Notably, neutrophils that are recruited to the lung and differentiate along Trajectory 2 (clusters 0, 6, 2, and 5) experience transcriptional reprogramming to acquire a heightened inflammatory phenotype (Fig. 5). In contrast to the canonical neutrophil differentiation pathway, including a short half-life, the infiltrated neutrophils in severe COVID-19 patients are transcriptionally active (Fig. 5b) in comparison to blood neutrophils and further differentiate into a hyper-inflammatory state (Fig. 5d). This is consistent with more recent reports of neutrophil transmigration in other respiratory illnesses such as cystic fibrosis[22], where neutrophils undergo lung/condition-specific adaptations upon recruitment from the circulation instead of the canonical rapid and transient effector function proceeding to cell death. Indeed, we observed increased expression of the interferon-stimulated gene (ISG) *IFI30*, followed by increased expression of *CCL3* (MIP-1α) and *CCL4* (MIP-1β) (Fig. 5d), which in turn can promote the recruitment of inflammatory monocytes to the lung and/or proinflammatory macrophage phenotypes in the airways. Strikingly, the neutrophils that are differentiating along Trajectory 2

further increase expression of *CXCL8* (IL-8) (Fig. 5d), perpetuating neutrophil recruitment to the lung.

We then investigated whether the recruited neutrophils or other cell types (i.e., myeloid, lymphoid, and stromal) in the airways of severe patients were productively infected with SARS-CoV-2. By including the SARS-CoV-2 genome sequence into our human reference transcriptome in the multi-omics single-cell analysis, we were able to assess viral mRNA transcripts at a single-cell level. Notably, we did not detect viral transcripts in any of the cell types in the airways of severe patients (Fig. S4a). This result is consistent with our viral plaque assays (Vero E6 cells) performed directly on the airway secretion. Whenever detected, the viral load was very low, even at 1:10 sample dilution (<10 plaques at 1:10 airway sample dilution) (Fig. S4b).

Collectively, the progressive increase in *IFI30, CCL3/4*, and *CXCL8* mRNA transcripts reveal a transcriptionally active state in neutrophils that is poised to sustain a hyperinflammatory milieu in the lung of severe COVID-19 patients even in the absence of viral load. Interestingly, we find that *CXCR4* expression, which has been attributed to immature neutrophils, is increased and sustained in mature lung-recruited neutrophils that differentiate along Trajectory 2 (Fig. 5d), possibly promoting survival and retention of pathogenic neutrophils in the lung. This is consistent with *CXCR4* expression dynamics previously detected in patients with cystic fibrosis[23].

Mature neutrophils are continuously recruited to the airways via the CXCL8/CXCR2 axis driven by lung neutrophils and monocytes

We next wanted to identify the potential cell receptor-ligand interactions that could be contributing to the recruitment of circulating neutrophils to the airways. We performed cell receptor-ligand interaction analysis (CellChat[24]) on combined total ETA cells and blood neutrophils and identified significant enrichment of the CXCL signaling network (Fig. 6a). Strikingly, our analysis reveals that all lung cell subsets utilize a similar CXCL signaling network to recruit a single subset of mature blood neutrophils, the blood cluster 2 (Fig. 6a). The robust lung recruitment of blood cluster 2 is largely orchestrated by the CXCL8 (IL-8)/CXCR2 axis, and to a lesser extent, by the CXCL2/CXCR2 axis (Fig. 6b-c). Of note, these results further support our finding that recent lung migrants (lung cluster 0) have the highest expression of *CXCR2* (Fig. 5c). Indeed, our analyses identified significant cell-cell communication between the lung neutrophil, myeloid and stromal populations, specifically with the CXCR2-expressing blood neutrophils (Fig. 6a). Virtually all lung neutrophils (particularly cluster 5), stromal cells, and monocytes show the potential to recruit circulating neutrophils (Fig. 6a), indicating a robust and redundant mechanism of neutrophil recruitment to the airways via the CXCL8/CXCR2 axis (Fig. 6b-c).

Notably, lung monocytes also have the potential to recruit circulating neutrophils (blood cluster 2) via a similar CXCL8/CXCR2 axis. In fact, as we showed above, the genetic reprogramming of lung infiltrating neutrophils leads to the production of the chemokines macrophage inflammatory

proteins (MIP) *CCL3* and *CCL4* (Fig. 5d). These neutrophil-derived chemokines can attract inflammatory monocytes from the circulation to the airways. Interestingly, the lung infiltrating monocytes also produce elevated levels of *CXCL8*, potentiating the recruitment of circulating neutrophils via the CXCL8/CXCR2 axis (Fig. 6b-c). Hence, both neutrophils and their recruited inflammatory monocytes in the airways exacerbate and sustain the pathogenic neutrophilia in the lungs of severe patients in a positive feedback loop.

Taken together, these findings implicate the CXCL pathway (specifically CXCL8 (IL-8)/CXCR2) as the predominant recruitment axis for neutrophils to the inflamed airways and further corroborate our Hi-D flow cytometry, gene expression, and secreted protein data analysis identifying IL-8 as the most abundant neutrophil-derived chemokine (and neutrophil chemotactic factor) in the airways of severe COVID-19 patients.

Discussion

Previous studies have reported increased neutrophilia in severe COVID-19 disease, particularly in the circulation[25, 26, 27]. In contrast, reports on exacerbated airway neutrophilia and the implication of lung neutrophils as the main cell type driving the acute respiratory distress syndrome (ARDS) in critically ill patients have not been conclusive, and the results have been somewhat variable[6, 7, 15, 28]. Here, we present the first comprehensive study of the lung immune response to SARS-CoV-2 in Black/AA individuals and unequivocally identify a robust and sustained airway neutrophilia that correlates with disease severity. The COVID-19 pandemic further highlighted some of the socio-economic and behavioral inequalities that may have contributed to troubling disparities in COVID-19-associated mortality, with almost 70% of deaths being Black/AA patients in some areas[1]. Although the socio-economic and behavioral differences indeed contribute to health disparities among demographics, a systematic investigation to determine the immunological features that characterize disease severity within Black/AA patients is notably lacking. Our studies here address this knowledge gap and suggest that in addition to current therapies, inhibiting neutrophil migration to the lung via CXCL8 (IL-8)/CXCR2 may represent an effective and targeted therapeutic approach for critically ill individuals that have been disproportionally affected by COVID-19.

Although previous studies on severe COVID-19 in humans have not been conclusive with regards to the role of airway neutrophilia in ARDS, studies in SARS-CoV-2-infected rhesus macaques and mice, where conditions and sample collection are more controlled, have identified exacerbated neutrophilia as a key immunological feature associated with disease severity[29, 30, 31]. Hence, taken together with previous studies on neutrophils[25, 26, 27, 7, 15, 28] along with animal models[29, 30, 31], our current findings provide compelling evidence that targeting exacerbated airway neutrophilia may constrain ARDS and prevent further lung damage in most patients requiring mechanical ventilator support. And although our studies represent one of the few targeted investigations in Black/AA patients, we believe our results have broader implications and are applicable to most patients.

Other immune cell types in the lung may contribute to the disease pathology in critically ill patients. In fact, the exacerbated numbers of neutrophils in the lung are likely to induce inflammatory signatures in other cell types that can potentiate disease severity. The myeloid lineage is the second most abundant cell type in the airways, after neutrophils, and is poised to influence disease progression. For example, we and others[32] have shown that infiltrating neutrophils sustain local production of calgranulins (S100A8/9/12), which can signal through and activate myeloid cells via TLR and RAGE receptors and compounding the already hyperinflammatory lung milieu. Interestingly, the inflammatory monocytes that are likely recruited to the lungs via neutrophil-secreted CCL3/4 also show elevated levels of neutrophil chemotactic factor IL-8, which helps sustain the recruitment of pathogenic neutrophils in a positive feedback loop. Further studies should determine the other effector functions of the myeloid and lymphoid subsets and how these cells interact with neutrophils to promote protection or disease pathology in the lungs of severe COVID-19 patients.

Interestingly, *CXCR4* is expressed and further upregulated in recruited neutrophils in severe patients (Figs. 4d, 4i, & 5d), which may promote neutrophil survival and retention during pneumonitis. CXCR4 expression on neutrophils is well described in terms of the CXCR4/CXCL12 chemotaxis for neutrophil release and trafficking from the bone marrow[33]. Although we do not find *CXCL12* mRNA transcripts in our scRNA-seq dataset, we were able to detect higher levels of CXCL12 protein in the airways of severe patients. However, not all severe patients show detectable levels of CXCL12 (SDF-1) protein in the airways, suggesting a wide distribution of this chemokine in the airways of severe patients. In contrast, we did observe the expression of *HMGB1* in the airways, which is an alternative ligand for CXCR4. Since the CXCL8/CXCR2 pathway is most notably increased and likely the primary neutrophil recruitment axis to the airways, we speculate that CXCR4 canonical signaling through HMGB1 or CXCL12 in the lung may promote neutrophil survival and retention at the site of inflammation, which has been previously reported[34]. Alternatively, CXCR4 signaling through the non-canonical ligand macrophage migration inhibitory factor (MIF) can stimulate de novo *CXCL8* expression, and subsequent IL-8 production[35], which we show is highly elevated in our severe disease cohort. These observations are aligned with our findings that recruited airway neutrophils sustain a transcriptionally active state, likely delaying cell death (~90% of the endotracheal aspirate cells were alive at the time of the assays).

In a prior study[36], we noted a similar pattern of CXCR4 expression on T cells (CD4+ and CD8+) from severe COVID-19 patients admitted to the ICU. We analyzed the phenotypic features of T cells from longitudinal specimens of mild and severe patients and observed that circulating T cells progressively decrease surface CXCR4 in severe patients that recovered and were discharged from the ICU. In contrast, ICU patients that succumbed to the disease showed a time-dependent escalation in activated bystander CXCR4+ T cells. We also observed that inflammatory CXCR4+ T cells are increased in the lungs of severe COVID-19 patients[36], suggesting that lung-homing inflammatory T cells may also contribute to immunopathology. Further investigation into the potential role of CXCR4 in cell survival, retention, or recruitment may unravel novel therapeutic targets to modulate inflammation and treat severe COVID-19.

Modulating inflammation through corticosteroids (particularly Dexamethasone) has shown clinical efficacy and is now the standard-of-care for patients progressing to severe COVID-19[37]. However, the pleiotropic effects of glucocorticoids and their propensity to cause neutrophilia are well documented in asthma and chronic obstructive pulmonary disease (COPD)[38]. Though a classical mechanism of action for Dexamethasone is transcriptional repression of proinflammatory cytokines, we observed very high levels of *CXCL8* and *IL1B* in addition to high concentrations of pulmonary and circulating IL-8 and IL-1β with prominent signatures by intracellular staining, particularly in airway neutrophils. Even beyond COVID-19, it has been shown that resolution of neutrophilia in ARDS has substantial prognostic benefit[9]. In contrast, IL-6 levels were lower than that of IL-8 and IL-1β in our patient cohort. Of note, overly abundant neutrophils were not producing as much IL-6 comparatively, which may explain, in part, why anti-IL-6/IL-6R studies failed to meet primary endpoints[39]. Here, were provide evidence of an uncoupled cytokine profile in airway fluids versus plasma where the lung microenvironment exhibits features of cytokine-induced ARDS driven largely by a proinflammatory, neutrophilic

feedforward loop. Notably, the CXCL8 (IL-8)/CXCR2 emerges as a key potential target for next-generation immunomodulatory therapy to reduce pathogenic neutrophilia and constrain severe disease in patients.

We also contend that recognizing the lung pathology in severe COVID-19 to be a neutrophilic and hyperinflammatory disease is paramount to achieve better outcomes in next-generation therapies. Although the lung pathology in COVID-19 is initiated by a viral infection, critically ill patients in the intensive care unit (ICU) no longer show signs of uncontrolled viral replication. In fact, not only did we not detect viral transcripts within the cells in the airways, plaque assays performed on the respiratory secretions from severe patients reveal significantly diminished if any, viral plaques from the endotracheal aspirates. This may explain, in part, why antiviral drugs such as Remdesivir were not able to prevent death when administered to critically ill patients in ICU[40].

Here, we present compelling evidence that neutrophils are poised to be the leukocyte population most responsible for the dysregulated hyperinflammatory response that drives ARDS in severe COVID-19 patients. Neutrophil frequency and inflammatory profiles reveal that neutrophils are not only the most abundant leukocyte population in the upper airways, but they are also producing the hallmark effector molecules associated with disease severity, including IL-8, IL-1β, and IL-6, along with potent proteases such as NE and MPO, which are inherently inflammatory and contribute to lung damage/pathology. Furthermore, we provide evidence of a neutrophil feedforward loop where IL-8, which is produced by virtually all airway neutrophils (and some myeloid and stromal cells), is the primary recruitment chemokine for circulating neutrophils and thereby potentiates neutrophilia in the inflamed airways.

Collectively, our findings implicate neutrophilia in the immunopathophysiology of severe COVID-19 disease where perpetual, transcriptionally active, and highly inflammatory pulmonary neutrophils drive ARDS despite a significantly low viral burden. Therapeutic intervention targeting neutrophil recruitment/retention at the site of inflammation has the potential to constrain ARDS in critically ill patients, particularly those most vulnerable to succumb to COVID-19.

Methods

Ethics and biosafety. A total of 35 individuals were recruited for this study. The 18 severe COVID-19+ patients were recruited from the Intensive Care Units of Emory University, Emory St. Joseph's, Emory Decatur, and Emory Midtown Hospitals. We also recruited 9 mild COVID-19-infected outpatients in the Emory Acute Respiratory Clinic, and 8 healthy adults from the Emory University Hospital. All studies were approved by the Emory Institutional Review Board (IRB) under protocol numbers IRB00058507, IRB00057983 and IRB00058271. Informed consent was obtained from the patients when they had decision making ability or from a legal authorized representative (LAR) if the patient was unable to provide consent. Blood and sputum or endotracheal aspirate (ETA) were obtained. Control blood samples were obtained from healthy adults matched by age and race. Study inclusion criteria included a confirmed COVID-19 diagnosis by PCR amplification of SARS-CoV-2 viral RNA obtained from nasopharyngeal or oropharyngeal swabs, age of 18 years or greater, and willingness and ability to provide informed consent. Exclusion criteria included a known history of autoimmune disease or malignancy for COVID-19+ subjects, and those with a confirmed history of COVID-19 diagnosis or COVID-19 vaccine were excluded from the healthy donor group. All work with infectious virus and respiratory samples from COVID-19 patients was conducted inside a biosafety cabinet within the Emory Health and Safety Office (EHSO)- and United States Department of Agriculture (USDA)-approved BSL3 containment facility in the Health Sciences Research Building at Emory University following protocols approved by the Institutional Biosafety Committee (IBC) and Biosafety Officer.

Patient sample collection and processing. Primary leukocytes from the airways of COVID-19 patients requiring mechanical ventilator support were collected bedside via endotracheal aspiration (ETA) and whole blood collected by standard venipuncture. Plasma from whole blood was isolated via centrifugation at 400 x g for 10 mins at 4˚C. To remove platelets, the isolated plasma was centrifuged at 4,000 x g for 10 mins at 4˚C. Untouched circulating leukocytes were isolated using the EasySep™ RBC Depletion Reagent (StemCell Technologies). ETA (from severe patients) or non-induced sputum (from mild patients) was mixed 1:1 with a 50mM EDTA solution in custom RPMI-1640 media deficient in biotin, L-glutamine, phenol red, riboflavin, and sodium bicarbonate (defRPMI-1640), with 3% newborn calf serum (final concentration 25 mM EDTA) and mechanically dissociated using a syringe to liberate leukocytes from mucins and other respiratory secretions. Supernatants were collected for further analysis, and cells passed through a 70 µm nylon strainer prior to counting and downstream processing.

High-dimensional 30-parameter flow cytometry. Cells (up to 10^7 total) were resuspended in defRPMI-1640 with 3% newborn calf serum and Benzonase™ (FACS buffer) in 5 mL FACS tubes and pre-incubated with GolgiStop™ (BD Biosciences) for 20 mins at 4˚C. Human TruStain FcX™ was then added, followed by a 10 min incubation at RT. The 24-color extracellular staining master mix (see Table S2) was prepared 2X in BD Horizon™ Brilliant Stain Buffer to prevent staining artifacts from BD Horizon Brilliant dye interactions and added 1:1 to cells, then incubated for 30 mins at 4˚C. Following staining (and total 1 h exposure to GolgiStop™), cells were washed with ~4 mL FACS buffer. The cells were resuspended in 200 µL of BD

Cytofix/Cytoperm™ fixation/permeabilization solution and incubated at 4˚C for 30 mins followed by a wash with ≥1 mL BD Perm/Wash™ Buffer. The 4-color intracellular staining (see Table S2) was prepared in BD Perm/Wash™ Buffer and cells stained for 30 mins at 4˚C. Cells were washed with ~4 mL BD Perm/Wash™ Buffer, then resuspended for a final 20 min incubation in 4% PFA and transported out of the BSL3 containment facility. Cells were washed in ~4 mL FACS buffer, then resuspended in 200-1000 µL for acquisition using BD FACSDiva™ Software on the Emory Pediatric/Winship Flow Cytometry Core BD FACSymphony™ A5. To distinguish auto-fluorescent cells from cells expressing low levels of a particular surface marker, we established upper thresholds for auto-fluorescence by staining samples with fluorescence-minus-one (FMO) control stain sets in which a reagent for a channel of interest is omitted. Data were analyzed with FlowJo™ v10.7 (FlowJo LLC).

Single-cell surface antibody-derived tag (ADT), encapsulation, and library generation. Leukocytes from whole blood and ETA samples were incubated with oligo-conjugated Ig-A/D/G/M for 10 mins at 4˚C followed by the addition of Human TruStain FcX™ (BioLegend) and 10 min incubation at RT. Cells were then surface stained with oligo-conjugated monoclonal antibody panel (total=89 see Table S3) for 30 min at 4˚C, followed by two washes in def-RPMI-1640/0.04% BSA. Cells were resuspended at a concentration of 1200-1500 cells/µL in def-RPMI-1640 /0.04% BSA and passed through a 20 or 40 µm cell strainer prior to loading onto a Chromium Controller (10XGenomics, Pleasanton, CA). Cells were loaded to target encapsulation of 10,000 cells. Gene expression and ADT libraries were generated using the Chromium Single Cell 5′ Library & Gel Bead Kit v1.1 with feature barcoding following the manufacturer's instructions. Gene expression (GEX) libraries were pooled and sequenced at a depth of approximately 540,000,000 reads per sample in a single S4 flow cell and ADT libraries at a depth of approximately 79,000,000 per sample in a single lane of an S4 flow cell on a NovaSeq™ 6000 (Illumina, San Diego, CA; see Table S4)

Multi-omics single-cell RNA sequencing (scRNA-seq). Single-cell 5′ unique molecular identifier (UMI) counting and barcode de-multiplexing were performed using CellRanger Software (v.5.0.0). To detect SARS-CoV-2 viral RNA reads, we built a custom reference genome from human GRCh38 and SARS-CoV-2 references (severe acute respiratory syndrome coronavirus 2 isolate Wuhan-Hu-1, complete genome, GenBank MN908947.3). Splicing-aware aligner STAR[41] was implemented to align FASTQ inputs to the reference genome, and the resulting files are automatically filtered by CellRanger to include only cell barcodes representing real cells. This determination is based on the distribution of UMI counts. ADT reads were aligned to a feature reference file containing the antibody-specific barcode sequences. To recover neutrophils, scRNA-seq UMI count matrices were imported to R 4.0.2, and data analyses were performed using Seurat v4.0[42]. We recovered neutrophils from CellRanger unfiltered count matrices by plotting surface CD16 ADT and CD66b ADT using the "FeatureScatter" function in Seurat. The double-positive barcodes were then extracted and further evaluated by GEX to confirm viable neutrophils as for other cell types described. A threshold for mitochondrial content per barcode was determined for each sample and applied as a cutoff to remove dead or dying cells (see Table S5). Most samples show high cell viability with a minimal proportion of dead cells.

The UMI counts of the GEX data were log-normalized by the “NormalizeData” function in Seurat prior to downstream analysis. Center log-ratio (CLR) transform in Seurat was performed on ADT UMIs when recovering neutrophils from the unfiltered matrices. For surface protein visualization and to classify major lineages, ADT UMIs were normalized using the R package Denoised and Scaled by Background[43] (DSB) to remove ambient UMI counts (i.e., background) prior to manual sequential gating by surface expression in SeqGeq v1.7 (FlowJo, LLC). DSB uses empty droplets to calculate background expression, which was manually selected according to the distribution of total ADT per cell in the raw count matrices (see Table S6). To minimize the influence from non-informative empty droplets, we removed cell barcodes with less than 100 total ADT UMIs before plotting the ADT distribution.

The standard Seurat workflow for GEX data was implemented on each sample, as previously described[42]. We classified major lineages based on a combination of gene transcript and surface protein detection, as in Fig. 4. Any cell barcodes within each major lineage that expressed markers exclusive to other major lineages were considered doublets and removed. In addition, we removed cell barcodes with extremely high total ADT UMIs, which we considered to be aggregated cells. To efficiently integrate replicate samples, we concatenated major lineages derived from the same tissue in different donors. We proceeded with data processing of replicates according to the workflow recommendations described in[44]. Briefly, samples were first treated individually as log normalized count matrices were scaled/Z-transformed, and the “vst” method of the Seurat function “FindVariableFeatures” was utilized to select the top 1000 highly variable genes of each sample. Highly variable genes shared between replicate samples were used to perform principal component analysis (PCA). To visualize the data, we performed UMAP reduction of the first 30 PCs, while in parallel, we applied the Leiden community detection algorithm at a resolution of 0.8. UMAPs for the integrated total Blood and integrated total ETA were generated by the standard Seurat 3 data integration workflow.

Receptor-ligand interaction and trajectory analyses. Clustered cells from lung and blood samples from each patient were investigated for evidence of intercellular communication using CellChat[24]. Clustered cell populations from the lung samples were combined with the blood neutrophils to determine which lung cell populations have the potential to recruit circulating neutrophils. The R package Slingshot was used to infer the trajectories of neutrophils recruited to the lungs. The cluster labels and the UMAP data inherited from the integrated ETA neutrophils were taken by the function “slingshot” to compute pseudotimes and trajectories. Clusters 0 and 5 were applied a posteriori as root and terminal nodes of the trajectories, respectively. Due to a risk of affecting the pseudotime data, the extension of trajectories was turned off. The default parameters include thresh = 0.001, stretch = 2, and shrink.method = “cosine”.

Mesoscale U-PLEX assays. U-PLEX Biomarker Group 1 Human Multiplex Assays (Meso Scale Discovery) were used to evaluate levels of 21 analytes in plasma and UVC-inactivated respiratory supernatants following the manufacturer's protocol (see Table S6). Samples were diluted 1:4 for all assays except for IL-8, MCP-1, and IL-1RA, which were above the upper limit

of detection for the assay and were diluted 1:100 to acquire measurement within the assay range. Final values were obtained by multiplying measurements by their respective dilution factor.

Myeloperoxidase (MPO) content and activity. The abundance and activity of MPO were quantified as previously described[21]. MPO activity and protein concentration were measured sequentially following the immunocapture. On average, across six 96-well plate assays, lower limits of quantification were 4.0 ng/mL (activity) and 0.84 ng/mL (protein). Samples above the lower limit of detection but below the lower limit of quantification were imputed as half of the latter, and those detected above the highest standard (50 ng/mL) at all dilutions were imputed as twice the standard concentration.

Plaque assays. Vero E6 cells were seeded in a 6-well plates (Falcon) with 5 x 10^5 cells/well in 5% DMEM 24 h prior to infection and checked to verify ≥80% confluency. 10-fold dilutions of virus, respiratory secretions, and/or scRNA-seq emulsion in serum-free DMEM (200 µL) were incubated on Vero E6 monolayers for 1 h absorption at 37˚C with rocking at 15 min intervals. After absorption, cells were overlain with 2% methylcellulose (MilliporeSigma) in 2% DMEM for 72 h at 37˚C in a 5% CO_2, humidified incubator. 72 h post-infection (hpi), methylcellulose was carefully removed, and cells gently rinsed once with 1X HBSS (Corning). Monolayers were fixed and plaques visualized with a solution of 0.4% Crystal Violet by weight in 80% methanol (MilliporeSigma) and 4% PFA (20% stock diluted in 1X HBSS; Electron Microscopy Sciences) for 20 mins at room-temperature (RT).

Statistical analyses. Statistical analyses were performed using GraphPad Prism9. Data were analyzed for distribution (normal (Gaussian) vs. lognormal) independently using the D'Agostino and Pearson test for normality in both the untransformed and Log10 transformed data. In cases where *N* was too small for D'Agostino and Pearson normality test, the Shapiro-Wilk test was used to assess distribution. When data passed both distribution tests, the likelihood of each distribution (normal vs. lognormal) was computed, and QQ-plots were generated for both untransformed, and Log10 transformed data. When Log10 transformed data had a higher likelihood of a normal distribution (passing normal distribution test) and/or failed lognormal distribution test, paired t-tests were performed for comparisons of matching blood and respiratory supernatant samples within a single group. If the data had unequal variance (as determined by an F-test on both the untransformed and Log10 transformed data), a ratio paired t-test was performed. All instances where lognormal distribution was more likely non-parametric Wilcoxon matched-pairs sign ranked tests were performed. For comparisons of the same sample type (blood or respiratory supernatant) across groups, unpaired t-tests were used, and if the data had unequal variance (as determined by an F-test), Welch's correction was applied (for normally distributed data) or a Mann-Whitney test to compare ranks (for data with a lognormal distribution). For comparisons across the three patient groups (i.e., healthy, mild-acute, severe), ordinary one-way ANOVA (if equal variance) or Brown-Forsythe and Welch ANOVA (if unequal variance) tests were performed for data with a normal distribution. Alternatively, data with a lognormal distribution were analyzed with a Kruskal-Wallis test.

Acknowledgments

This study was funded by NIH/NIAID R01AI123126 (EEBG) and R01AI123126-05S1 (EEBG), NIH T32-HL116271-07 (RPR), the Program for Breakthrough Biomedical Research, and Lowance Center for Human Immunology. We thank Keivan Zandi, Ann Chahroudi, Nils Schoof, Kira Moresco, and Stacy Heilman of the Department of Pediatrics, Emory University, for their assistance with setting up the BLS3 facility and kindly providing SARS-CoV-2 viral stocks. We thank Nadia Roan (Gladstone Institutes/UCSF) and Sulggi Lee (UCSF) for helpful discussions. Flow cytometry data were collected at the Emory's Pediatrics/Winship Flow Cytometry Core (access supported in part by Children's Healthcare of Atlanta). We acknowledge the Genomic Cores at Yerkes Non-Human Primate Research Center at Emory University (NIH P51 OD011132; NIH S10 OD026799), Baylor College of Medicine, and the Parker H. Petit Institute for Bioengineering and Bioscience at the Georgia Institute of Technology for the single-cell library sequences. We are grateful for the efforts of Sang N. Le, John Varghese, Anum Jalal Saeyun Lee, and Rahul Patel who also contributed to patient recruitment. We also thank the nurses, staff, and providers in the 71 ICU in Emory University Hospital Midtown, the medical ICU in Emory Decatur Hospital, the 5G/6G ICU in Emory University Hospital, and the ICU in Emory Saint Joseph's Hospital without whom our work would not have been possible. We thank all of the healthy individuals, patients, and their families for their participation in this study.

References

1. Van Dyke, M.E. *et al.* Racial and ethnic disparities in COVID-19 incidence by age, sex, and period among persons aged< 25 years—16 US jurisdictions, January 1–December 31, 2020. *Morbidity and Mortality Weekly Report* **70**, 382 (2021).

2. Lucas, C. *et al.* Longitudinal analyses reveal immunological misfiring in severe COVID-19. *Nature* **584**, 463-469 (2020).

3. Merad, M. & Martin, J.C. Pathological inflammation in patients with COVID-19: a key role for monocytes and macrophages. *Nature Reviews Immunology* **20**, 355-362 (2020).

4. Olwal, C.O. *et al.* Parallels in Sepsis and COVID-19 Conditions: Implications for Managing Severe COVID-19 Patients. *Frontiers in immunology* **12**, 91 (2021).

5. Carvalho, T., Krammer, F. & Iwasaki, A. The first 12 months of COVID-19: a timeline of immunological insights. *Nature Reviews Immunology* **21**, 245-256 (2021).

6. Bost, P. *et al.* Deciphering the state of immune silence in fatal COVID-19 patients. *Nature communications* **12**, 1-15 (2021).

7. Liao, M. *et al.* Single-cell landscape of bronchoalveolar immune cells in patients with COVID-19. *Nature medicine*, 1-3 (2020).

8. Liang, W. *et al.* Development and validation of a clinical risk score to predict the occurrence of critical illness in hospitalized patients with COVID-19. *JAMA Internal Medicine* (2020).

9. Steinberg, K.P. *et al.* Evolution of bronchoalveolar cell populations in the adult respiratory distress syndrome. *American journal of respiratory and critical care medicine* **150**, 113-122 (1994).

10. Barnes, B.J. *et al.* Targeting potential drivers of COVID-19: Neutrophil extracellular traps. *Journal of Experimental Medicine* **217** (2020).

11. Kong, M., Zhang, H., Cao, X., Mao, X. & Lu, Z. Higher level of neutrophil-to-lymphocyte is associated with severe COVID-19. *Epidemiology & Infection* **148** (2020).

12. Liu, Y. *et al.* Neutrophil-to-lymphocyte ratio as an independent risk factor for mortality in hospitalized patients with COVID-19. *Journal of Infection* (2020).

13. Schulte-Schrepping, J. *et al.* Severe COVID-19 is marked by a dysregulated myeloid cell compartment. *Cell* **182**, 1419-1440 (2020).

14. Silvin, A. *et al.* Elevated calprotectin and abnormal myeloid cell subsets discriminate severe from mild COVID-19. *Cell* (2020).

15. Grant, R.A. *et al.* Circuits between infected macrophages and T cells in SARS-CoV-2 pneumonia. *Nature* **590**, 635-641 (2021).

16. Wilk, A.J. *et al.* A single-cell atlas of the peripheral immune response in patients with severe COVID-19. *Nature medicine* **26**, 1070-1076 (2020).

17. Kreutmair, S. *et al.* Distinct immunological signatures discriminate severe COVID-19 from non-SARS-CoV-2-driven critical pneumonia. *Immunity* (2021).

18. Ren, X. *et al.* COVID-19 immune features revealed by a large-scale single-cell transcriptome atlas. *Cell* **184**, 1895-1913 e1819 (2021).

19. Xu, G. *et al.* The differential immune responses to COVID-19 in peripheral and lung revealed by single-cell RNA sequencing. *Cell Discov* **6**, 73 (2020).

20. Forrest, O.A. *et al.* Frontline Science: Pathological conditioning of human neutrophils recruited to the airway milieu in cystic fibrosis. *Journal of leukocyte biology* **104**, 665-675 (2018).

21. Chandler, J.D. *et al.* Myeloperoxidase oxidation of methionine associates with early cystic fibrosis lung disease. *European Respiratory Journal* **52** (2018).

22. Margaroli, C. *et al.* Transcriptional firing represses bactericidal activity in cystic fibrosis airway neutrophils. *Cell Reports Medicine* **2**, 100239 (2021).

23. Makam, M. *et al.* Activation of critical, host-induced, metabolic and stress pathways marks neutrophil entry into cystic fibrosis lungs. *Proc Natl Acad Sci U S A* **106**, 5779-5783 (2009).

24. Jin, S. *et al.* Inference and analysis of cell-cell communication using CellChat. *Nature communications* **12**, 1-20 (2021).

25. Bohn, M.K. *et al.* Pathophysiology of COVID-19: Mechanisms Underlying Disease Severity and Progression. *Physiology (Bethesda)* **35**, 288-301 (2020).

26. Meizlish, M.L. *et al.* A neutrophil activation signature predicts critical illness and mortality in COVID-19. *Blood Adv* **5**, 1164-1177 (2021).

27. Metzemaekers, M. *et al.* Kinetics of peripheral blood neutrophils in severe coronavirus disease 2019. *Clin Transl Immunology* **10**, e1271 (2021).

28. Wauters, E. *et al.* Discriminating mild from critical COVID-19 by innate and adaptive immune single-cell profiling of bronchoalveolar lavages. *Cell Res* **31**, 272-290 (2021).

29. Guo, Q. *et al.* Induction of alarmin S100A8/A9 mediates activation of aberrant neutrophils in the pathogenesis of COVID-19. *Cell Host Microbe* **29**, 222-235 e224 (2021).

30. Hoang, T.N. *et al.* Baricitinib treatment resolves lower-airway macrophage inflammation and neutrophil recruitment in SARS-CoV-2-infected rhesus macaques. *Cell* **184**, 460-475 e421 (2021).

31. Vanderheiden, A. *et al.* CCR2-dependent monocyte-derived cells restrict SARS-CoV-2 infection. *bioRxiv* (2021).

32. Silvin, A. *et al.* Elevated Calprotectin and Abnormal Myeloid Cell Subsets Discriminate Severe from Mild COVID-19. *Cell* **182**, 1401-1418 e1418 (2020).

33. Martin, C. *et al.* Chemokines acting via CXCR2 and CXCR4 control the release of neutrophils from the bone marrow and their return following senescence. *Immunity* **19**, 583-593 (2003).

34. Yamada, M. *et al.* The increase in surface CXCR4 expression on lung extravascular neutrophils and its effects on neutrophils during endotoxin-induced lung injury. *Cellular & molecular immunology* **8**, 305-314 (2011).

35. Pawig, L., Klasen, C., Weber, C., Bernhagen, J. & Noels, H. Diversity and Inter-Connections in the CXCR4 Chemokine Receptor/Ligand Family: Molecular Perspectives. *Front Immunol* **6**, 429 (2015).

36. Neidleman, J. *et al.* Distinctive features of SARS-CoV-2-specific T cells predict recovery from severe COVID-19. *medRxiv* (2021).

37. Group, R.C. Dexamethasone in hospitalized patients with Covid-19. *New England Journal of Medicine* **384**, 693-704 (2021).

38. Ronchetti, S., Ricci, E., Migliorati, G., Gentili, M. & Riccardi, C. How glucocorticoids affect the neutrophil life. *International journal of molecular sciences* **19**, 4090 (2018).

39. Mullard, A. Anti-IL-6Rs falter in COVID-19. *Nature reviews. Drug discovery* **19**, 577 (2020).

40. Beigel, J.H. *et al.* Remdesivir for the Treatment of Covid-19 - Final Report. *N Engl J Med* **383**, 1813-1826 (2020).

41. Dobin, A. *et al.* STAR: ultrafast universal RNA-seq aligner. *Bioinformatics* **29**, 15-21 (2013).

42. Hao, Y. *et al.* Integrated analysis of multimodal single-cell data. *bioRxiv* (2020).

43. Mulè, M.P., Martins, A.J. & Tsang, J.S. Normalizing and denoising protein expression data from droplet-based single cell profiling. *bioRxiv* (2020).

44. Babcock, B.R. *et al.* Optimized data matrix normalization minimizes batch-specific systemic variation in scRNA-seq data. *BioRxiv* (2021).

45. Shaath, H., Vishnubalaji, R., Elkord, E. & Alajez, N.M. Single-Cell Transcriptome Analysis Highlights a Role for Neutrophils and Inflammatory Macrophages in the Pathogenesis of Severe COVID-19. *Cells* **9** (2020).

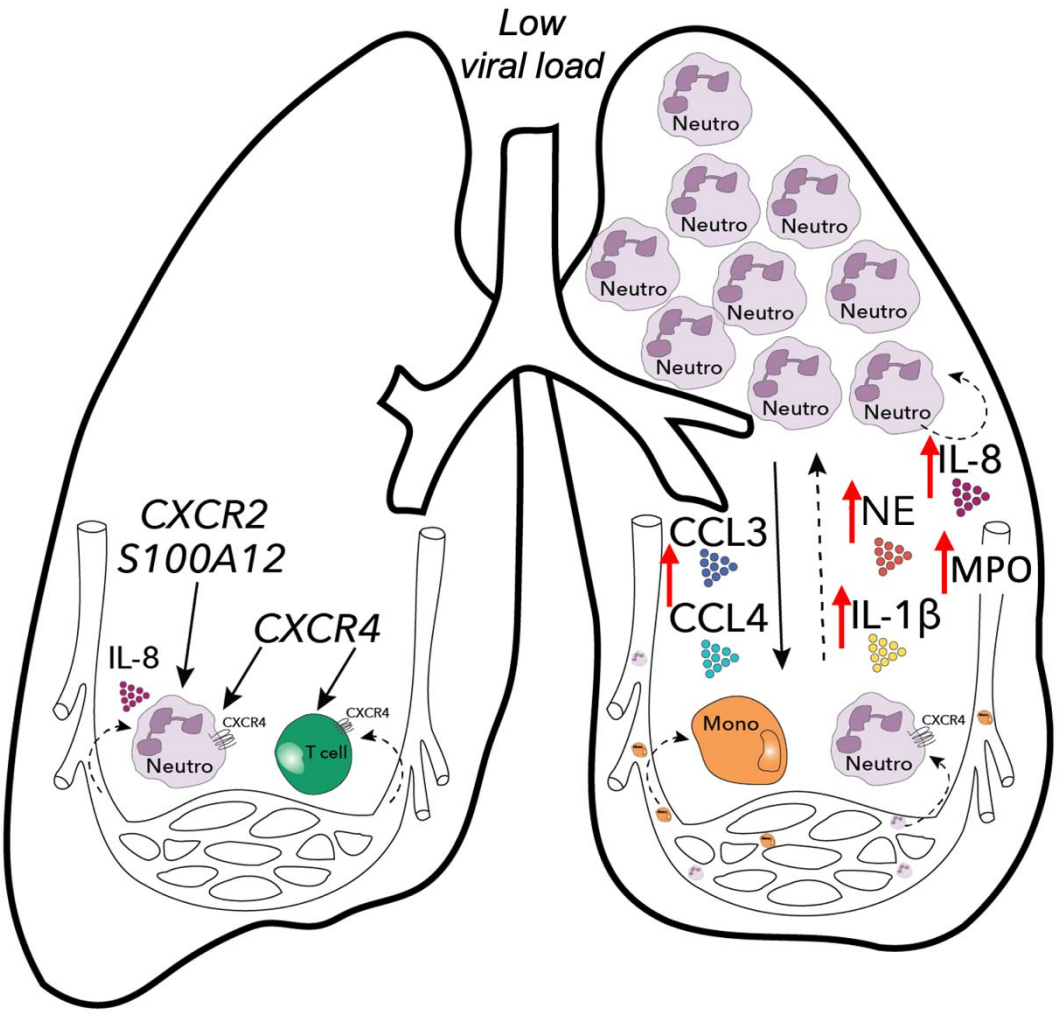

Graphical Abstract

The lung pathology due to severe COVID-19 is marked by a perpetual pathogenic neutrophilia, leading to acute respiratory distress syndrome even in the absence of viral burden. Circulating neutrophils are recruited to the airways via IL-8 (CXCL8)/CXCR2 chemotaxis. Recently migrated mature neutrophils further differentiate into a transcriptionally active and hyperinflammatory state, with an exacerbated expression of IL-8 (CXCL8), IL-1β, CCL3, CCL4, neutrophil elastase (NE), and myeloperoxidase (MPO) activity. Airway neutrophils and recruited inflammatory monocytes further increase their production of CXCL8, perpetuating lung neutrophilia in a feedforward loop.

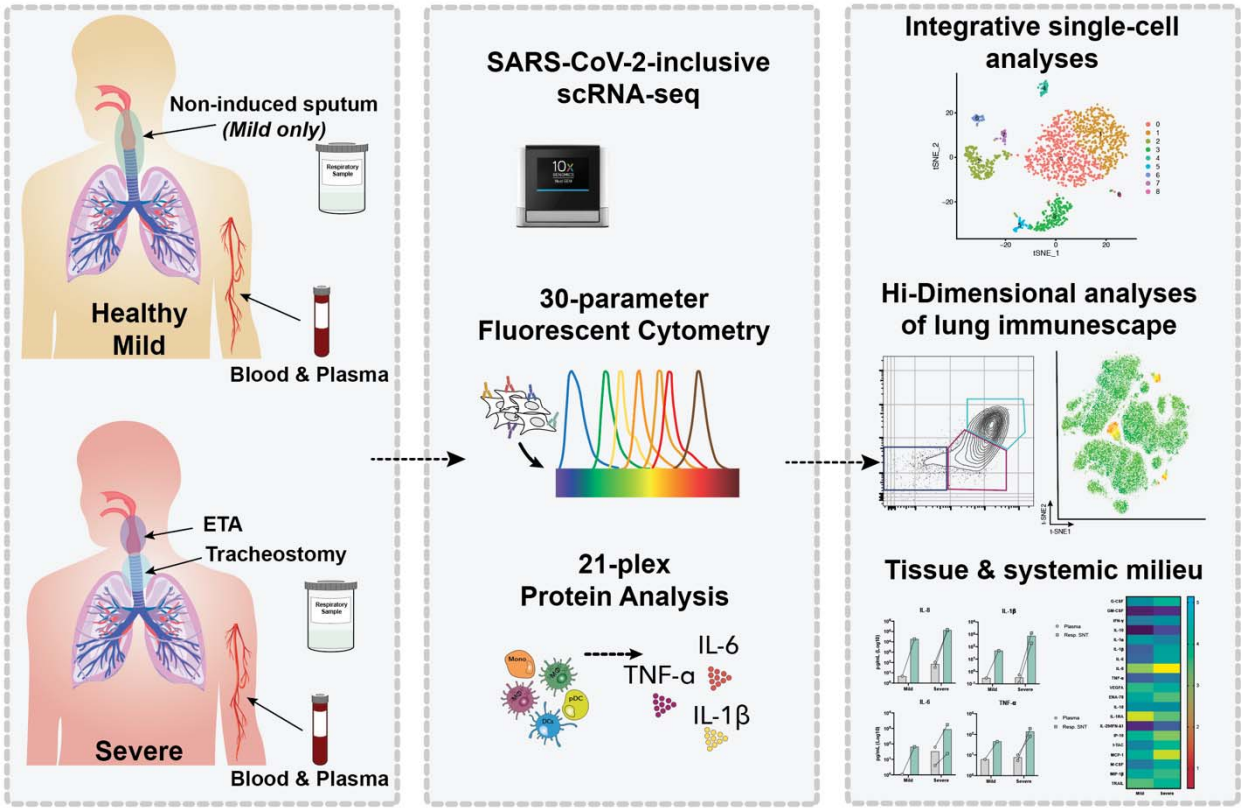

Figure 1. ***Experimental design for the systems immunology approach (integrated multi-omics single-cell assays) to study COVID-19 patient samples***. Respiratory samples (sputum or endotracheal aspirates) and matching blood from all subjects were collected for analysis by 21-plex Mesoscale analysis, high-dimensional (Hi-D) 30-parameter flow cytometry, and multi-omics scRNA-seq. Cells from endotracheal aspirates (ETA) and blood of severe COVID-19 patients along with blood from healthy individuals were surface-stained with a panel of 89 oligo-conjugated monoclonal antibodies prior to single-cell encapsulation, and analyses were performed with a custom human reference genome that included the SARS-CoV-2 genome to simultaneously detect viral mRNA transcripts. Integrative multi-omics analyses were performed on the resulting data sets.

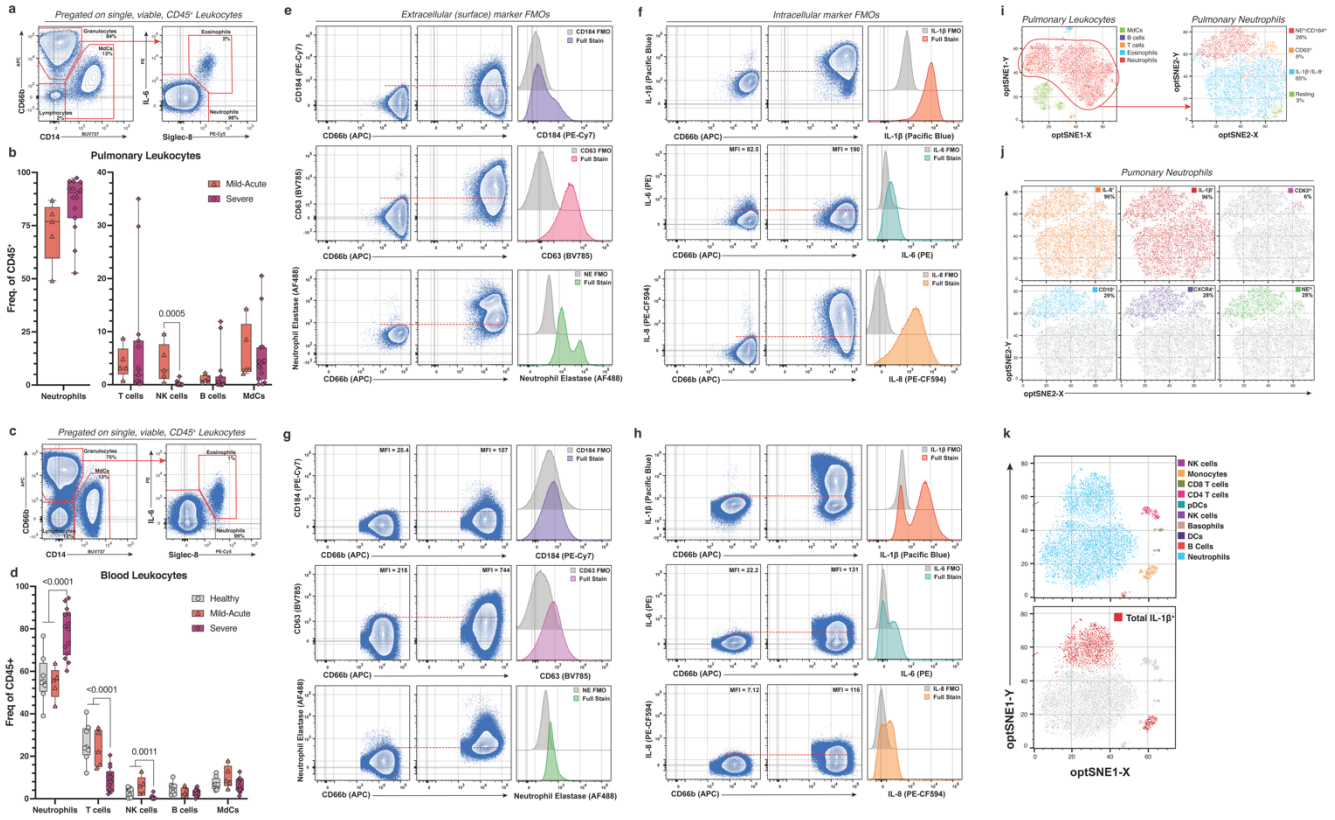

Figure 2. ***Exacerbated neutrophilia in the airways and matching blood of severe COVID-19 patients.*** Gating strategy and box plots show distributions of leukocytes isolated from endotracheal aspirates (ETA) (a & b) and whole blood (c & d) from severe patients. FMOs and representative stains for extracellular (e & g) and intracellular (f & h) markers were used to evaluate neutrophil phenotype by Hi-D flow cytometry. Representative opt-SNE projections of Hi-D flow cytometry data for total pulmonary leukocytes (ETA) and neutrophils (i). Pulmonary neutrophils were isolated and representative opt-SNE projections (j) for markers that revealed neutrophil inflammatory phenotype. Representative opt-SNE projections of Hi-D flow cytometry data of total circulating leukocytes from severe patients and intracellular IL-1β+ cells (k). MdCs = myeloid-derived cells. For comparisons across the three patient groups (i.e., healthy, mild-acute, severe), ordinary one-way ANOVA (if equal variance) or Brown-Forsythe and Welch ANOVA (if unequal variance) tests were performed for data with a normal distribution, and data with a lognormal distribution were analyzed with a Kruskal-Wallis test.

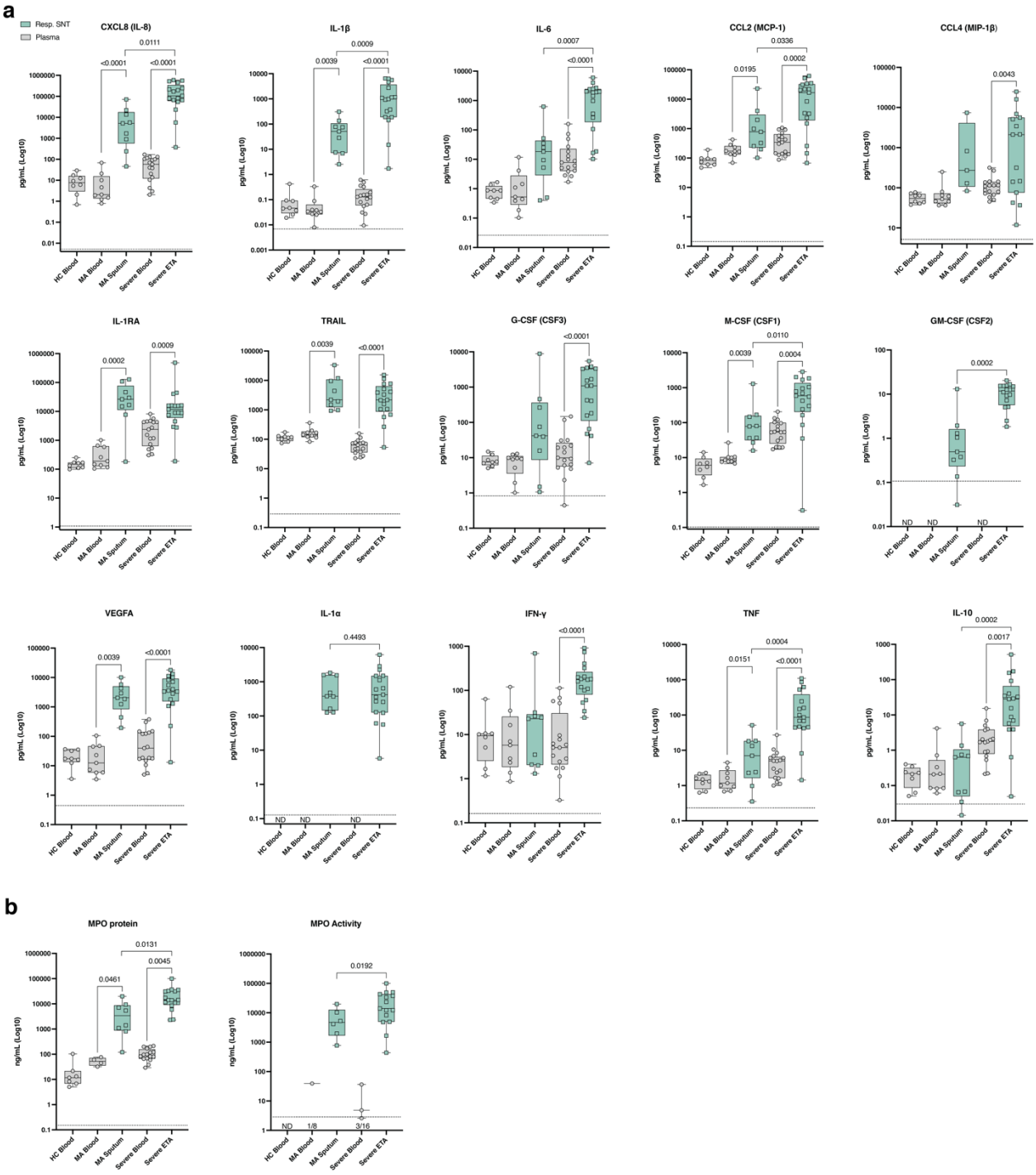

Figure 3. ***Cytokine release syndrome is dominated by IL-8 and IL-1β with pronounced myeloperoxidase content and activity in the lung microenvironment***. (a) Concentration (pg/mL) of 15 analytes interrogated by Mesoscale analyses in plasma (gray circles) and respiratory supernatant (Resp. SNT; green squares) from healthy control (HC), mild-acute (MA), and severe COVID-19 patients. (b) Concentration (ng/mL) of myeloperoxidase (MPO) protein and MPO activity in plasma vs. Resp. SNT. Dotted line = assay limit of detection (LOD).

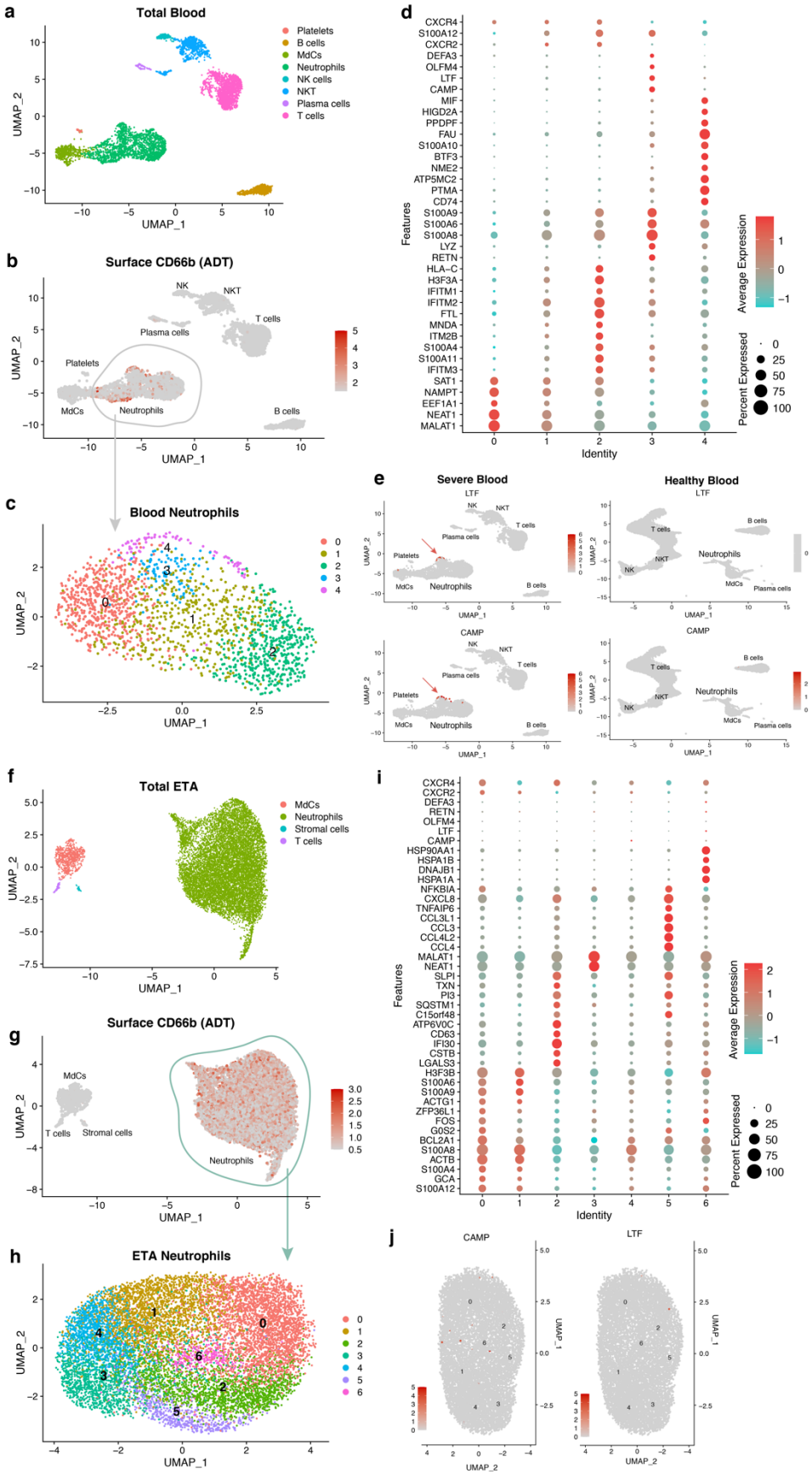
a
Total Blood
Platelets
B cells
MdCs
Neutrophils
NK cells
NKT
Plasma cells
T cells
UMAP_1
UMAP_2
b
Surface CD66b (ADT)
NK
NKT
T cells
Plasma cells
Platelets
MdCs
Neutrophils
B cells
c
Blood Neutrophils
d
Features
Identity
Average Expression
Percent Expressed
e
Severe Blood
Healthy Blood
LTF
CAMP
f
Total ETA
MdCs
Neutrophils
Stromal cells
T cells
g
Surface CD66b (ADT)
h
ETA Neutrophils
i
j
CAMP
LTF

801

Figure 4. ***Multi-omic single-cell RNA-seq reveals emergency granulopoiesis in the circulation and abundant heterogeneous population of mature neutrophils in the airways with distinct inflammatory state.*** UMAP visualization of scRNA-seq of total integrated blood (a) and endotracheal aspirate (ETA) (f) cells. Major cell lineages were identified by surface protein expression (ADT: antibody-derived tags). Neutrophils were identified based on surface CD66b (b & g), and total neutrophils were subclustered for further analysis (c & h). Dot plots of the intersection of the top differentially expressed genes in neutrophil clusters (d & i) sorted by average log-fold change for blood (c) and lung (h) neutrophils, respectively. UMAP visualization of signature genes of immature neutrophils in blood (e) and lung (j) of severe patients.

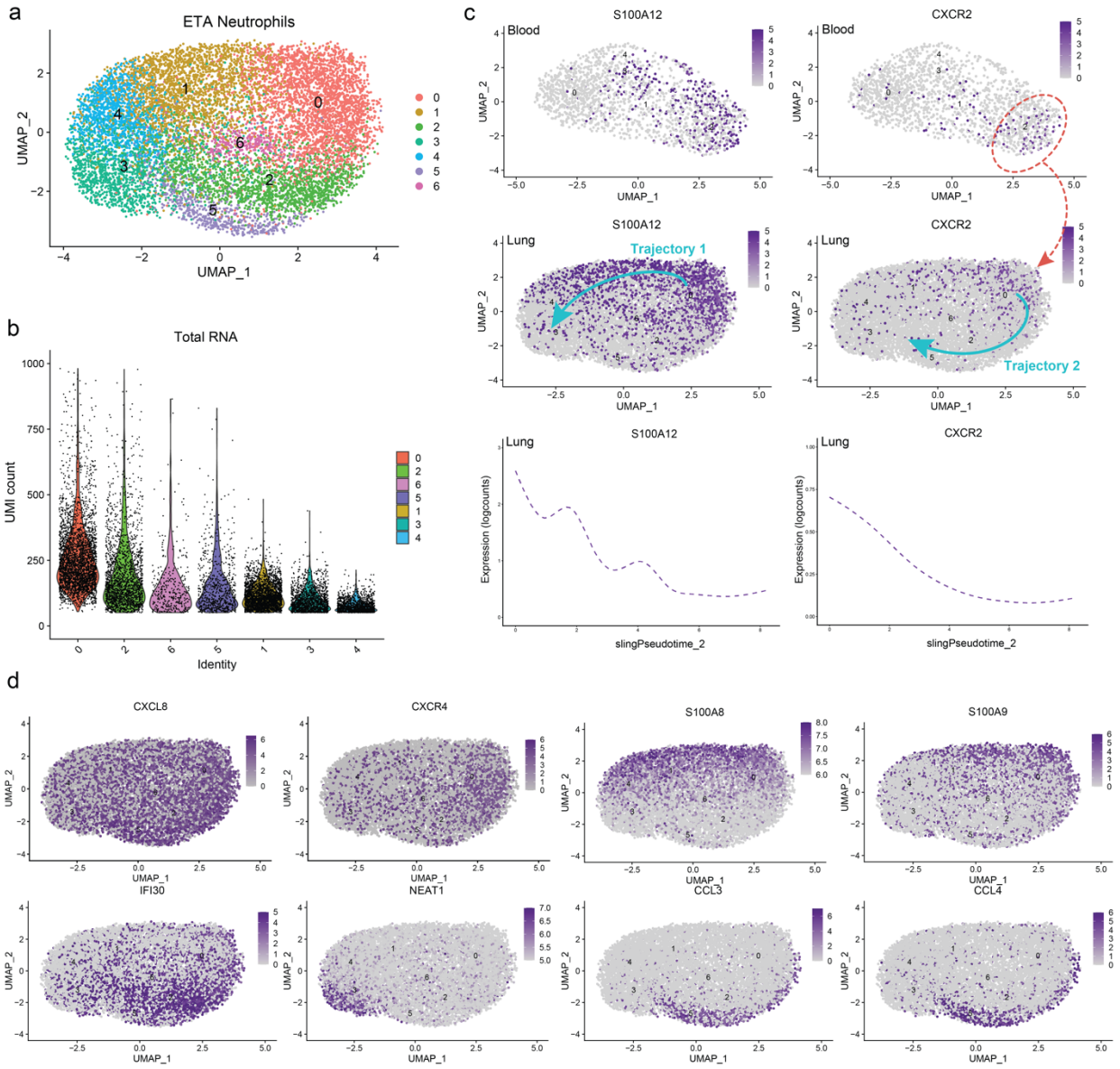

Figure 5. ***Recruited airway neutrophils are transcriptionally active and progress toward a hyperinflammatory state***. Integrated airway neutrophils (a) show marked variation in mRNA abundance (b), which correlates with progression toward a hyper inflammatory state (c & d). *S100A12* and *CXCR2* mark a cluster of mature neutrophils in the blood (c) that likely represents the neutrophil subset recruited to the lung. Cell Trajectory analysis (Slingshot) identifies two potential pathways (Trajectories 1 and 2) for recently migrated neutrophils (blue arrows in c), where expression of *S100A12* and *CXCR2* decline along these trajectories (c). Neutrophils recruited to the lung acquire a hyperinflammatory profile along Trajectory 2 (d), characterized by high expression of *CXCR4,* interferon-stimulated gene (ISG) *IFI30*, macrophage inflammatory protein (MIP) *CCL3* and *CCL4*, and exacerbated increase in *CXCL8* (IL-8) (d).

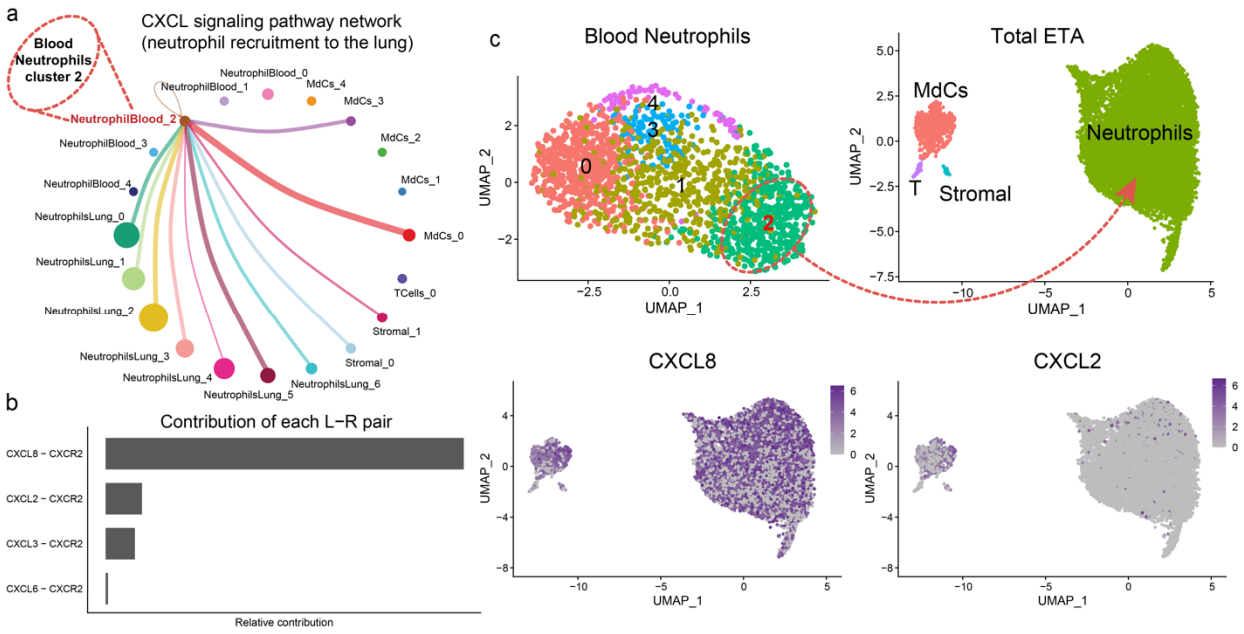

Figure 6. ***Mature neutrophils are continuously recruited from circulation by lung neutrophils, myeloid and stromal cells via the CXCL8 (IL-8)/CXCR2 axis.*** Cell receptor-ligand pair analyses (CellChat[24]) from scRNA-seq data identify significant CXCL signaling pathway network enrichment between lung cells and blood neutrophils. Blood neutrophil cluster 2 represents the main subset potentially recruited to the lung (a). Recruitment of blood cluster 2 (a & c) is largely orchestrated by the CXCL8 (IL-8)/CXCR2 axis, and to a lesser extent, by the CXCL2/CXCR2 axis (b & c). MdCs: Myeloid-derived Cells.

Supplemental Material:

#	Demographic	PID	Status	Sex	Age Group	Dexamethasone or equivalent	Remdesivir (No. of doses)	Date intubated	Date PCR positive Dx	Date sample collected	Length ICU stay (days)
1	AA	PHA0036	Critical	Male	18-34	Yes	2	12/31/2020	1/10/2021	2/2/2021	42
2	AA	PHA0001	Critical	Male	35-54	Yes	0	6/8/2020	6/9/2020	6/17/2020	32
3	AA	PHA0004	Critical	Male	35-54	Yes	0	7/18/2020	7/11/2020	8/5/2020	37
4	AA	PHA0006	Critical	Male	35-54	Yes	0	8/16/2020	8/11/2020	8/20/2020	8
5	AA	PHA0018	Critical	Male	35-54	Yes	2	9/29/2020	10/14/2020	10/8/2020	13
6	AA	PHA0041	Critical	Male	35-54	Yes	2	2/6/2021	2/6/2021	2/10/2021	14
7	AA	PHA0003	Critical	Male	55+	Yes	2	6/25/2020	6/23/2020	6/30/2020	14
8	A	PHA0008	Critical	Male	55+	Yes	2	8/30/2020	8/29/2020	9/3/2020	19
9	AA	PHA0024	Critical	Male	55+	Yes	2	12/31/2020	12/27/2020	1/6/2021	9
10	AA	PHA0025	Critical	Male	55+	Yes	0	12/24/2020	12/20/2020	1/8/2021	26
11	AA	PHA0031	Critical	Male	55+	Yes	1	1/24/2021	1/23/2021	1/27/2021	11
12	AA	PHA0032	Critical	Male	55+	Yes	1	1/14/2020	1/9/2021	1/27/2021	40
13	AA	PHA0035	Critical	Male	55+	Yes	0	1/20/2021	1/18/2021	2/2/2021	53
14	AA	PHA0002	Critical	Female	55+	Yes	0	6/20/2020	6/20/2020	6/24/2020	25
15	AA	PHA0005	Critical	Female	55+	Yes	0	7/18/2020	7/16/2020	8/12/2020	33
16	AA	PHA0007	Critical	Female	55+	Yes	0	8/10/2020	8/9/2020	9/2/2020	60
17	AA	PHA0010	Critical	Female	55+	Yes	2	9/21/2020	9/17/2020	9/24/2020	18
18	AA	PHA0026	Critical	Female	55+	Yes	1	12/28/2020	12/27/2020	1/8/2021	16
19	A	PHA0040	Mild-Acute	Male	35-54	Yes	0	N/A	1/6/2021	2/8/2021	N/A
20	AA	PHA0043	Mild-Acute	Male	35-54	Yes	0	N/A	Unclear	2/18/2021	N/A
21	AA	PHA0023	Mild-Acute	Male	55+	Yes	0	N/A	11/6/2020	11/11/2020	N/A
22	AA	PHA0047	Mild-Acute	Male	55+	Yes	0	N/A	2/8/2021	2/19/2021	N/A
23	AA	PHA0012	Mild-Acute	Female	35-54	Yes	0	N/A	9/18/2020	9/29/2020	N/A
24	AA	PHA0013	Mild-Acute	Female	35-54	Yes	0	N/A	9/21/2020	9/29/2020	N/A
25	AA	PHA0044	Mild-Acute	Female	35-54	Yes	0	N/A	2/16/2021	2/19/2021	N/A
26	AA	PHA0046	Mild-Acute	Female	35-54	Yes	0	N/A	2/12/2021	2/19/2021	N/A
27	AA	PHA0045	Mild-Acute	Female	55+	Yes	0	N/A	2/12/2021	2/19/2021	N/A
28	AA	PHA1009	Healthy	Female	18-34	Yes	0	N/A	N/A	10/23/2020	N/A
29	AA	PHA1005	Healthy	Female	35-54	Yes	0	N/A	N/A	10/23/2020	N/A
30	AA	PHA1006	Healthy	Female	35-54	Yes	0	N/A	N/A	10/23/2020	N/A
31	AA	PHA1007	Healthy	Female	35-54	Yes	0	N/A	N/A	10/23/2020	N/A
32	AA	PHA1008	Healthy	Female	35-54	Yes	0	N/A	N/A	10/23/2020	N/A
33	AA	PHA1010	Healthy	Female	35-54	Yes	0	N/A	N/A	10/23/2020	N/A
34	AA	PHA1011	Healthy	Female	35-54	Yes	0	N/A	N/A	2/10/2021	N/A
35	AA	PHA1012	Healthy	Female	55+	Yes	0	N/A	N/A	2/17/2021	N/A

Table S1. ***Demographic and clinical data from the 35 Black/African American individuals enrolled in our studies.***

a CoV-Neutrophil

	Laser	Detector	Antigen	Fluorophore	Clone	Isotype	Vendor	Cat. No.	Titration
1	488 nm	B 515/20	Neutrophil elastase (NE)	FITC	950317	Mouse IgG1, κ	R&D Systems	IC91671G	1:25
2		B 610/20	CD45-RA	BB630	HI-100	Mouse IgG2a, κ	BD Biosciences	624294	1:160
3		B 670/30	CD11b	BB660	ICRF44	Mouse IgG1, κ	BD Biosciences	624295	1:50
4		B 710/50	CD45	BB700	HI-30	Mouse IgG1, κ	BD Biosciences	746090	1:640
5		B 750/30	CD4	BB755	RPA-T4	Mouse IgG1, κ	BD Biosciences	624391	1:100
6		B 780/60	HLA-DR (MHC II)	BB790	G46-6	Mouse IgG2a, κ	BD Biosciences	624296	1:50
7	405 nm	V 431/28	CD163	BV421	GHI/6I	Mouse IgG1, κ	BioLegend	333612	1:25
8		V 470/15	IL-1β	Pacific Blue	H1b-98	Mouse IgG1, κ	BioLegend	511710	1:20
9		V 586/15	CD56	BV570	HCD56	Mouse IgG1, κ	BioLegend	318330	1:100
10		V 610/20	CD86	BV605	FUN-1	Mouse IgG1, κ	BD Biosciences	562999	1:50
11		V 670/30	TNF	BV650	MAb11	Mouse IgG1, κ	BD Biosciences	563418	1:80
12		V 710/50	CD19	BV711	HIB19	Mouse IgG1, κ	BioLegend	302246	1:20
13		V 740/35	CD16 (FcγRIII)	BV750	3G8	Mouse IgG1, κ	BD Biosciences	747461	1:320
14		V 780/60	CD63 (LAMP-3)	BV785	H5C6	Mouse IgG1, κ	BioLegend	353044	1:80
15	561 nm	YG 586/15	IL-6	PE	MQ2-13A5	Rat IgG1, κ	BD Biosciences	554545	1:20
16		YG 610/20	IL-8 (CXCL8)	PE-CF594	G265-8	Mouse IgG2b, κ	BD Biosciences	563531	1:20
17		YG 670/30	Siglec-8	PE-Cy5	7C9	Mouse IgG1, κ	BioLegend	347114	1:100
18		YG 710/50	CD10	PE-Cy5.5	HI10a	Mouse IgG1, κ	Homemade	—	1:40
19		YG 780/60	CD184	PE-Cy7	12G5	Mouse IgG2a, κ	BioLegend	306514	1:40
20	355 nm	UV 379/28	CD64 (FcγRI)	BUV395	10.1	Mouse IgG1, κ	BD Biosciences	740300	1:80
21		UV 450/50	GhostDye (Viability)	UV450	—	—	Tonbo Biosciences	13-0868-T500	1:100
22		UV 586/15	CD172a/b (SIRPα/β1)	BUV563	SE5A5	Mouse IgG1, κ	BD Biosciences	748435	1:10
23		UV 670/30	CD123 (IL-3Rα)	BUV661	9F5	Mouse IgG1, κ	BD Biosciences	741628	1:40
24		UV 740/35	CD14	BUV737	M5E2	Mouse IgG2a, κ	BD Biosciences	612763	1:50
25		UV 820/60	CD3ε	BUV805	SK1	Mouse IgG1, κ	BD Biosciences	612889	1:40
26	640 nm	R 670/30	CD66b	APC	QA17A51	Mouse IgG1, κ	BioLegend	396906	1:200
27		R 710/50	CD11c	AF700	Bu15	Mouse IgG1, κ	BioLegend	337220	1:200
28		R 780/60	CD32 (FcγRII)	APC-Fire750	FUN-2	Mouse IgG2b, κ	BioLegend	303220	1:400

b CoV-Global Distributions

	Laser	Detector	Antigen	Fluorophore	Clone	Isotype	Vendor	Cat. No.	Titration
1	488 nm	B 515/20	CD45	FITC	HI-30	Mouse IgG1, κ	BioLegend	304017	1:160
2	405 nm	V 610/20	CD8α	BV605	SK1	Mouse IgG1, κ	BioLegend	344742	1:20
3		V 670/30	HLA-DR (MHC II)	BV650	L243	Mouse IgG2a, κ	BioLegend	307650	1:50
4		V 710/50	CD4	BV711	RPA-T4	Mouse IgG1, κ	BioLegend	300558	1:40
5		V 740/35	CD16 (FcγRIII)	BV750	3G8	Mouse IgG1, κ	BD Biosciences	747461	1:320
6		V 780/60	CD19	BV785	HIB19	Mouse IgG1, κ	BioLegend	302240	1:40
7	561 nm	YG 586/15	CD123 (IL-3Rα)	PE	6H6	Mouse IgG1, κ	BioLegend	306006	1:400
8		YG 670/30	Siglec-8	PE-Cy5	7C9	Mouse IgG1, κ	BioLegend	347114	1:100
9		YG 710/50	CD14	PE-Fire700	63D3	Mouse IgG1, κ	BioLegend	367158	1:100
10		YG 780/60	CD11c	PE-Cy7	Bu-15	Mouse IgG1, κ	BioLegend	337216	1:160
11	355 nm	UV 450/50	GhostDye (Viability)	UV450	—	—	Tonbo Biosciences	13-0868-T500	1:100
12	640 nm	R 670/30	CD11b	APC	ICRF44	Mouse IgG1, κ	BioLegend	301350	1:400
13		R 710/50	CD3ε	AF700	HIT3a	Mouse IgG2a, κ	BioLegend	300324	1:320
14		R 780/60	CD66b	APC-Fire750	QA17A51	Mouse IgG1, κ	BioLegend	396908	1:80

Table S2. ***High-dimensional 30-parameter flow cytometry panels, including intracellular cytokine staining, used for airway and blood cells.*** Flow cytometer configuration and cytometry reagents used in the final panels to interrogate (a) neutrophil phenotype and (b) global immune cell distributions and blood and ETA samples. Monoclonal antibody (mAb) master mixes were prepared in brilliant stain buffer and samples stained as described in the methods section. Titrations of all reagents were determined in house for each lot independently prior to use. BB: Brilliant Blue, BV: Brilliant Violet, PE: Phycoerytherin, BUV: Brilliant Ultraviolet, APC: Allophycocyanin, AF: AlexaFluor, FITC: Fluorescein isothiocyanate.

	Antigen	Clone	Vendor	Cat. No.
1	CD10	HI10a	Biolegend	312233
2	CD101 (BB27)	BB27	Biolegend	331017
3	CD103 (Integrin αE)	Ber-ACT8	Biolegend	350233
4	CD107a (LAMP-1)	H4A3	Biolegend	328649
5	CD117 (c-kit)	104D2	Biolegend	313243
6	CD11b	ICRF44	Biolegend	301359
7	CD11c	S-HCL-3	Biolegend	371521
8	CD123	6H6	Biolegend	306045
9	CD127 (IL-7Rα)	A019D5	Biolegend	351356
10	CD133	S16016B	Biolegend	394007
11	CD137	4B4-1	Biolegend	309839
12	CD138 (Syndecan-1)	MI15	Biolegend	356539
13	CD14	M5E2	Biolegend	301859
14	CD15 (SSEA-1)	W6D3	Biolegend	323053
15	CD16	3G8	Biolegend	302065
16	CD161	HP-3G10	Biolegend	339947
17	CD163	GHI/61	Biolegend	333637
18	CD169	7-239	Biolegend	346021
19	CD183 (CXCR3)	G025H7	Biolegend	353747
20	CD184 (CXCR4)	12G5	Biolegend	306533
21	CD185 (CXCR5)	J252D4	Biolegend	356939
22	CD19	HIB19	Biolegend	302265
23	CD196 (CCR6)	G034E3	Biolegend	353440
24	CD197 (CCR7)	G043H7	Biolegend	353251
25	CD1c	L161	Biolegend	331547
26	CD1d	51.1	Biolegend	350319
27	CD20	2H7	Biolegend	302363
28	CD206	15-2	Biolegend	321147
29	CD209 (DC-SIGN)	9E9A8	Biolegend	330121
30	CD21	Bu32	Biolegend	354923
31	CD23	EBVCS-5	Biolegend	338525
32	CD24	ML5	Biolegend	311143
33	CD25	BC96	Biolegend	302649
34	CD269 (BCMA)	19F2	Biolegend	357523
35	CD27	O323	Biolegend	302853
36	CD274 (B7-H1, PD-L1)	29E.2A3	Biolegend	329751
37	CD275 (B7-H2, ICOSL)	2D3	Biolegend	309419
38	CD279 (PD-1)	EH12.2H7	Biolegend	329963
39	CD28	CD28.2	Biolegend	302963
40	CD29 (Integrin B1)	TS2/16	Biolegend	303029
41	CD3	UCHT1	Biolegend	300479
42	CD307d (FcRL4)	413D12	Biolegend	340213
43	CD307e (FcRL5)	509f6	Biolegend	340309
44	CD309 (VEGFR2)	7D4-6	Biolegend	359921
45	CD32	FUN-2	Biolegend	303225
46	CD324	67A4	Biolegend	324127
47	CD326 (EpCAM)	9C4	Biolegend	324247
48	CD335 (NKp46)	9.00E+02	Biolegend	331941
49	CD370 (CLEC9A)	8F9	Biolegend	353809
50	CD38	HIT2	Biolegend	303543
51	CD4	RPA-T4	Biolegend	300567
52	CD40	5C3	Biolegend	334348
53	CD41	HIP8	Biolegend	303739
54	CD44	BJ18	Biolegend	338827
55	CD45	2D1	Biolegend	368545
56	CD45R/B220	RA3-6B2	Biolegend	103273
57	CD45RA	HI100	Biolegend	304163
58	CD45RO	UCHL1	Biolegend	304259
59	CD49a	TS2/7	Biolegend	328319
60	CD5	UCHT2	Biolegend	300637
61	CD56 (NCAM)	QA17A16	Biolegend	392425
62	CD62L	DREG-56	Biolegend	304851
63	CD64	10.1	Biolegend	305045
64	CD66b	6/40c	Biolegend	392909
65	CD69	FN50	Biolegend	310951
66	CD80	2D10	Biolegend	305243
67	CD86	IT2.2	Biolegend	305447
68	CD8a	RPA-T8	Biolegend	301071
69	CD95 (Fas)	DX2	Biolegend	305651
70	CX3CR1	K0124E1	Biolegend	355705
71	HLA-DR	L243	Biolegend	307663
72	IgD	IA6-2	Biolegend	348245
73	IgG	M1310G05	Biolegend	410727
74	IgM	MHM-88	Biolegend	314547
75	Ig light chain κ	MHK-49	Biolegend	316533
76	Ig light chain λ	MHL-38	Biolegend	316629
77	Siglec-8	7C9	Biolegend	347115
78	TCR Vα7.2	3C10	Biolegend	351735
79	TCR γ/δ	B1	Biolegend	331231
80	TIGIT (VSTM3)	A15153G	Biolegend	372729
81	XCR1	S15046E	Biolegend	372617
	Custom oligo-conjugated in-house			
82	ACE2	535919	Sino Biological	MAB9332-100
83	CD160	BY55	Biolegend	341202
84	CD16b	2D2G5B9	Sino Biological	11046-MM01
85	CD178	NOK-1	Biolegend	306402
86	CD34	581	Biolegend	343602
87	CD43	CD43-10G7	Biolegend	343202
88	CD9	HI9a	Biolegend	312102
89	IgA	IS11-8E10	Myltenyi	130-093-073

Table S3. ***Panel of oligo-conjugated antibodies used in multi-omics scRNA-seq assays to measure surface protein markers on cells from airways and blood.*** A total of 89 oligo-conjugated antibody-derived tags (ADT) were used to evaluate surface protein expression of target antigens via scRNA-seq. Reagents no. 82-89 were not commercially available in the TotalSeq-C™ format, so custom oligo-conjugated reagents were generated in-house using purified monoclonal antibodies and commercially available 5' Feature Barcode Antibody Conjugation - Lightning-Link® kits (abcam). Cell surface marker expression of major lineage markers were used to help cluster/validate gene expression data as described in the methods.

		PID	Total reads	Mean reads/cell
ETA	GEX	PHA0007	593,835,060	350,345
		PHA0008	555,825,992	2,241,234
		PHA0010	587,153,474	872,442
		PHA0018	541,561,148	459,729
	ADT	PHA0007	85,070,531	2,101
		PHA0008	78,647,311	7,514
		PHA0010	46,042,783	2,989
		PHA0018	73,265,461	5,399
Blood	GEX	PHA0007	518,672,044	273,129
		PHA0008	540,400,013	641,044
		PHA0010	592,394,112	543,980
		PHA0018	556,699,985	1,484,533
		PHA1005	541,306,254	158,787
		PHA1006	501,896,927	200,198
		PHA1007	512,999,099	172,902
		PHA1008	506,988,059	160,898
		PHA1009	527,201,752	130,463
		PHA1010	480,796,663	332,042
	ADT	PHA0007	74,597,277	2,115
		PHA0008	80,175,737	1,536
		PHA0010	62,927,249	1,067
		PHA0018	79,818,668	1,395
		PHA1005	77,435,258	1,145
		PHA1006	88,850,369	1,334
		PHA1007	88,329,209	1,169
		PHA1008	93,579,790	1,351
		PHA1009	91,162,676	1,281
		PHA1010	89,597,131	1,251

Table S4. ***Sequencing depth of independent samples.*** All samples gene expression (GEX) libraries were pooled and run in a single S4 flow cell on a NovaSeq™ 6000. All antibody-derived tag (ADT) libraries were pooled and sequenced in a single lane of a S4 flow cell on a NovaSeq™ 6000. Total reads and mean number of reads per cell for both GEX and ADT are reported for each sample independently, with average read per sample reported in the methods.

PID	Blood (%)	ETA (%)
PHA0007	30	30
PHA0008	20	25
PHA0010	10	25
PHA0018	30	25
PHA1005	30	
PHA1006	30	
PHA1007	30	
PHA1008	20	
PHA1009	20	
PHA1010	25	

Table S5. ***Mitochondrial gene thresholds.*** Threshold for mitochondrial gene distribution (percentage) for each sample used to exclude potential dead cells in scRNA-seq data. Threshold was evaluated and set for each sample independently.

PID	Blood (Total ADT UMI)	ETA (Total ADT UMI)
PHA0007	125–500	125–1250
PHA0008	125–1000	125–1250
PHA0010	125–1500	125–750
PHA0018	125–1500	125–1000
PHA1005	125–1250	
PHA1006	125–1250	
PHA1007	125–1500	
PHA1008	125–1500	
PHA1009	125–1500	
PHA1010	125–1500	

Table S6. ***Distribution of antibody-derived tag (ADT) data*****.** The distribution of total ADT UMIs was determined and recorded per each sample independently.

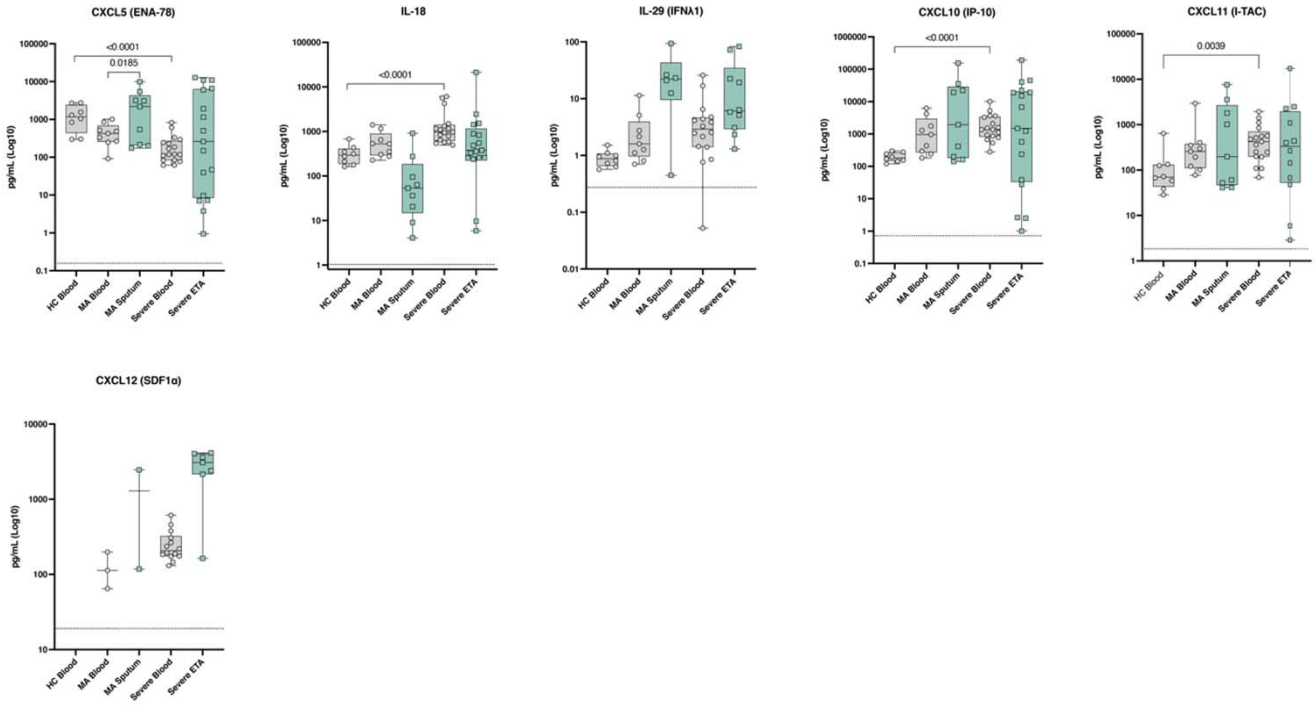

Figure S1. ***Additional cytokine assessment in blood and lungs*****.** Concentration (pg/mL) of remaining 6 analytes interrogated by Mesoscale analyses in plasma (gray circles) and respiratory supernatant (Resp. SNT; green squares). Dotted line = assay limit of detection (LOD).

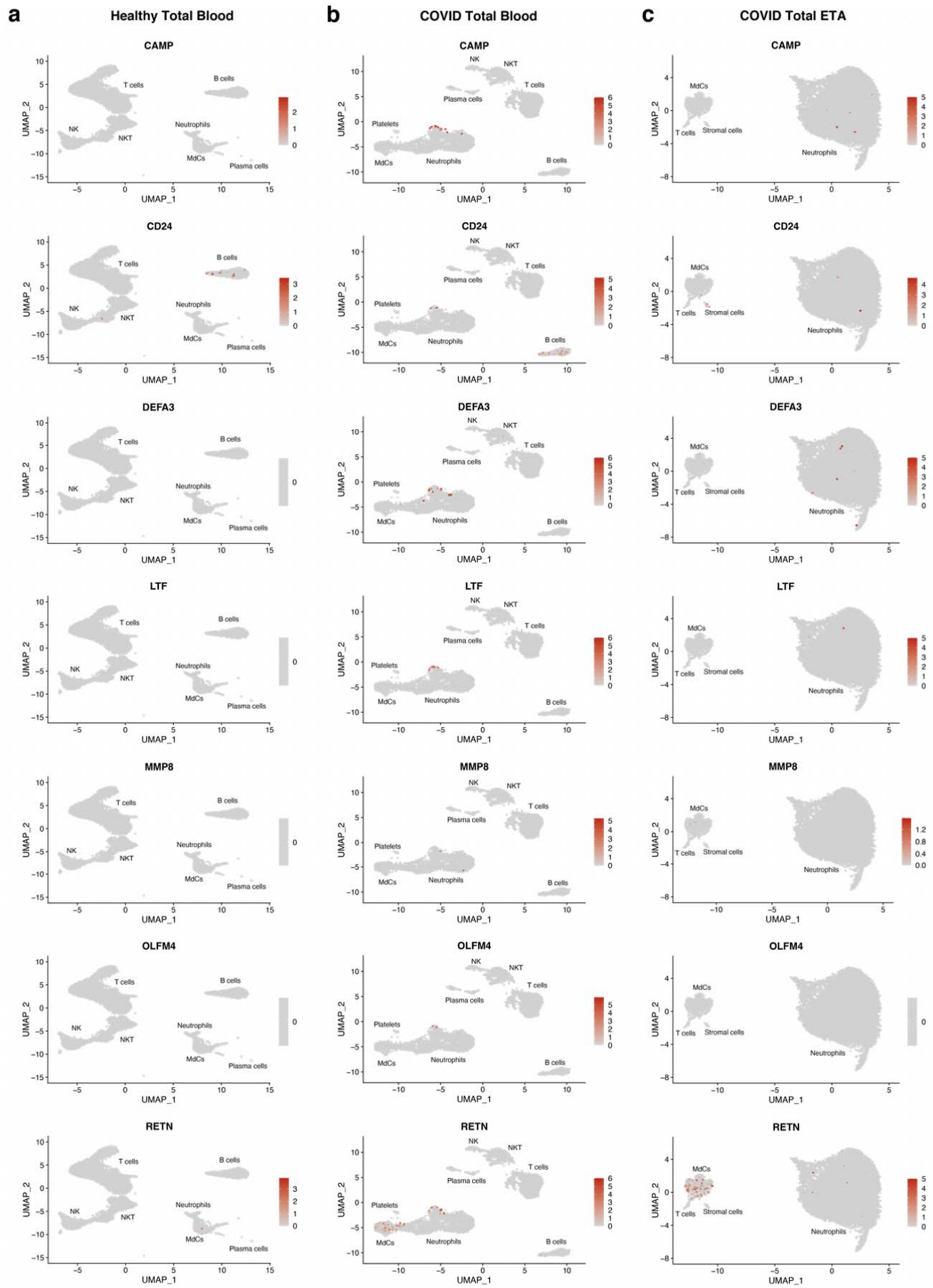
a
Healthy Total Blood
b
COVID Total Blood
c
COVID Total ETA
CAMP
CD24
DEFA3
LTF
MMP8
OLFM4
RETN
UMAP_1
UMAP_2
T cells
B cells
NK
NKT
Neutrophils
MdCs
Plasma cells
Platelets
Stromal cells

886

Figure S2. ***Gene signature for immature neutrophils is lacking in healthy donors and lungs of COVID19 patients*****.** UMAP visualizations of genes that identify immature neutrophils in the blood healthy individuals (a) and severe COVID-19 patients (b), along with cells from the lungs of severe COVID-19 patients (c).

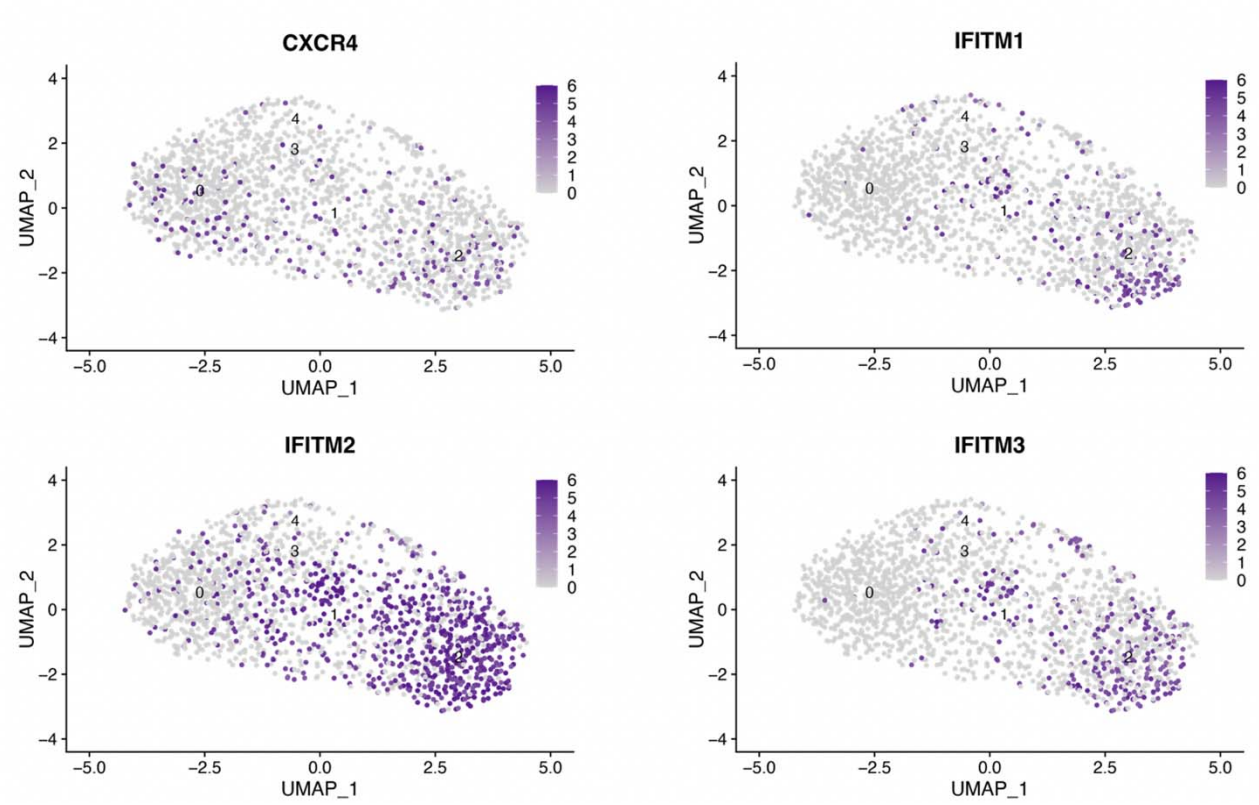

Figure S3. ***Putative population of blood neutrophils recruited to the lung during COVID-19 pathogenesis*****.** Blood neutrophils from COVID-19 patients were clustered independently and UMAP visualizations of differential expression of *CXCR4* in cluster 2 along with genes associated with an inflammatory response and previously described[45] in neutrophils from COVID-19 patients.

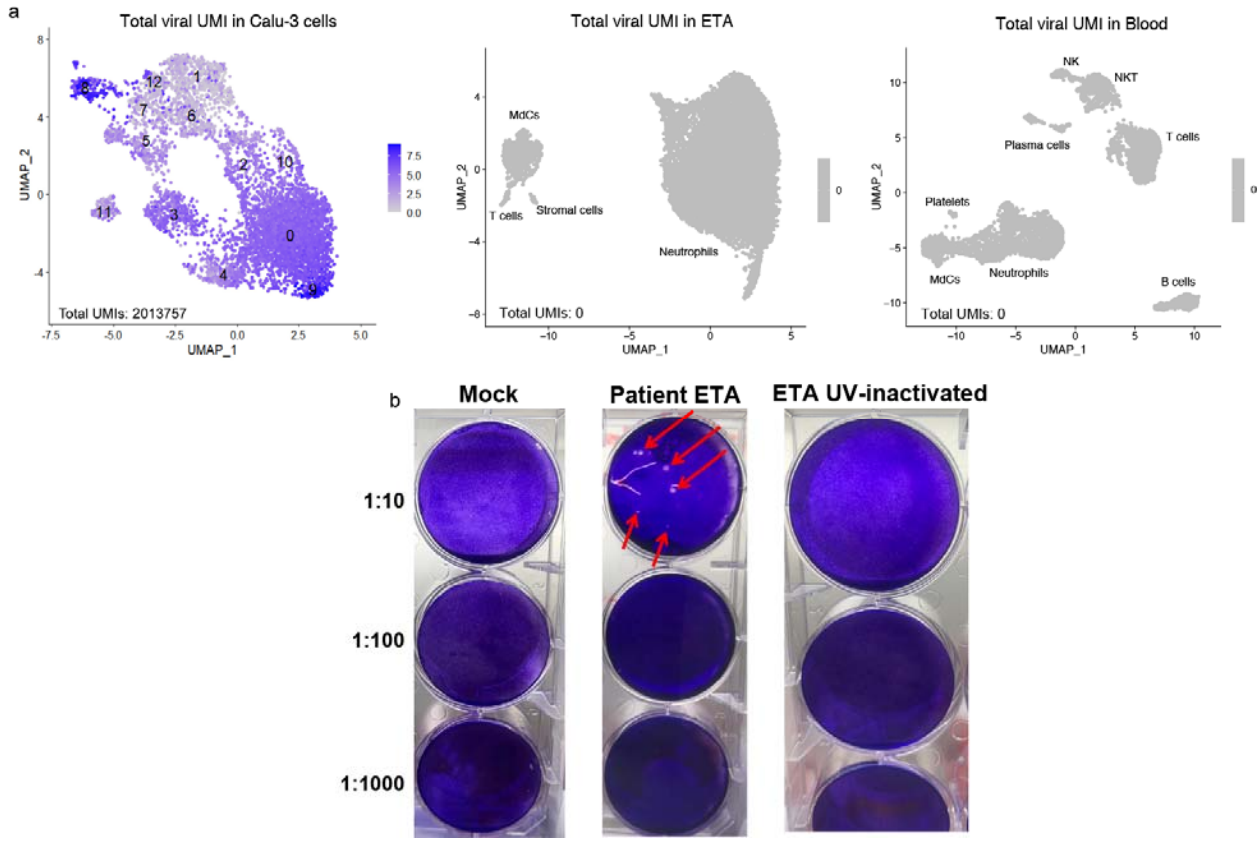

Figure S4. ***Viral transcripts (scRNA-seq) and viral plaques in the airways of severe patients.*** Calu-3 cells were infected with SARS-CoV-2 and encapsulated for scRNA-seq assays (a) following the same protocol used for patient cells. Millions of viral transcripts (UMI) were detected in about 5,000 cells. The same virus-inclusive scRNA-seq assay was performed on both airway and matching blood samples from severe COVID-19 patients (a, second and third panels). We did not detect any level of viral transcripts in the cells from severe patients (total UMI = 0). The respiratory secretion from severe patients was diluted 1:10, 1:100, and 1:1000 and plated on Vero E6 cells for viral plaque assay (b). Whenever detectable, the viral load was significantly lower. Middle column (b) shows representative of a positive patient with six detectable plaques in 1:10 dilution.